Inflammation (2026) 49:18
https://doi.org/10.1007/s10753-025-02361-x

RESEARCH

Lactate and H3K18 Lactylation Contribute To the Exacerbation of Acute Pancreatitis by Modulating NCOA4-mediated Ferroptosis

Zi-Yu Han[1] · Xue-Ying Ma[1] · Shi-Ya Ma[1] · Zhao-jian Shen[1] · Zhong-Hua Lu[1] · Yun Sun[1] · Wei-Li Yu[1]

Received: 19 June 2025 / Revised: 24 November 2025 / Accepted: 25 November 2026
© The Author(s) 2025

Abstract

Elevated lactate levels have been linked to poor prognosis in patients with acute pancreatitis (AP). Lactate-derived lactylation, a novel post-translational modification, has been implicated in various pathological processes by modulating gene transcription. However, the molecular mechanisms by which lactate and lactylation contribute to the pathogenesis of AP remain incompletely understood. An in vivo model of AP was established by intraperitoneal injection of L-arginine. Changes in both Pan- and histone-specific lysine lactylation levels were assessed using western blotting and immunofluorescence. The effects of exogenous lactate supplementation or inhibition of lactate production on pancreatic injury, inflammation, and ferroptosis were evaluated. Target genes regulated by H3K18 lactylation (H3K18la) during ferroptosis were identified through CUT&Tag, RNA sequencing (RNA-seq), ChIP-qPCR, and luciferase reporter assays. For NCOA4 knockdown, AAV-sh-NCOA4 and NCOA4-specific siRNA were utilized. In an in vitro AP model using AR42J pancreatic acinar cells treated with various drugs and siRNA, mitochondrial membrane potential (MMP), intracellular ferrous iron, and reactive oxygen species (ROS) levels were measured. Lactate levels in AP were significantly elevated and positively correlated with inflammation and pancreatic tissue injury. Both Pan- and histone lysine lactylation, particularly H3K18la, were significantly increased. H3K18la was markedly enriched at the NCOA4 promoter region. Exogenous lactate increased H3K18la expression, elevated ferrous iron and ROS levels, reduced MMP in pancreatic acinar cells, thereby promoting ferroptosis, exacerbating inflammation, and aggravating pancreatic tissue injury. However, lactate production inhibition exerted the opposite effects. The activity of NCOA4 promoter was enhanced by Lac-Na, but suppressed by si-EP300 and oxamate. Knockdown of NCOA4 using either AAV-sh-NCOA4 or si-NCOA4 effectively alleviated lactate-promoted ferroptosis, inflammation, and pancreatic injury. Our findings suggest that lactate and H3K18la exacerbate inflammation and tissue injury in AP by modulating NCOA4-mediated ferroptosis. These findings provide novel insights into the molecular mechanisms underlying AP pathogenesis.

Keywords Acute pancreatitis · Ferroptosis · Lactylation · H3K18la · NCOA4

Introduction

Acute pancreatitis (AP) is one of the leading causes for hospitalization due to digestive diseases. It originates from the abnormal activation of pancreatic trypsin within the pancreatic acinar cells, which leads to inflammatory damage of the pancreatic tissue [1–5]. The incidence, mortality and recurrence rates of AP are high, imposing a significant financial burden on patients and potentially causing long-term complications, including diabetes and exocrine pancreatic insufficiency [6–9]. Currently, treatment methods for AP are limited, and there is a lack of drug interventions targeting the underlying mechanisms of the disease [3, 10, 11]. Therefore, conducting a comprehensive study on the pathogenesis

Zi-Yu Han and Xue-Ying Ma contributed equally to this work.

✉ Yun Sun
sunyunicu@163.com

✉ Wei-Li Yu
ywl7026@mail.ustc.edu.cn

[1] The First Department of Critical Care Medicine, The Second Affiliated Hospital of Anhui Medical University, Hefei 230601, China

Published online: 29 December 2025

of AP and the development of targeted and effective treatment strategies are crucial for timely intervention, slowing down the progression of the disease, and improving the prognosis of patients.

Clinical evidence indicates that AP patients often present elevated lactate levels. The increase in lactate concentrations is an independent risk factor for organ failure and mortality in AP patients [12–15]. Lactate levels usually exhibit a positive correlation with disease severity [16, 17]. Recently, a new type of post-translational modification termed lactylation. Derived from lactate, has been reported to regulate gene transcription by binding to the promoters of target genes, thereby playing vital roles in tumor progression as well as macrophage polarization [18–22]. A recent study revealed that lactate enhances H3K18 lactylation (H3K18la) at the METTL3 promoter, modulating m6A methylation and subsequently promoting ACSL4 expression, which induces ferroptosis and exacerbates acute lung injury associated with sepsis [23], suggesting a potential link between lactate, H3K18la, lung injury and ferroptosis. To date, the mechanism by which high lactate-induced pancreatic injury during AP onset is not completely clear.

During the onset of AP, cytokine storms triggered by the release of multiple cytokines are closely related to regulated cell death and plays a pivotal role in the pathophysiology of AP [3, 24]. Ferroptosis is a unique form of regulated cell death characterized by iron-dependent polyunsaturated fatty acid peroxidation and an increase in reactive oxygen species (ROS) [25, 26]. Ferroptosis can be regulated by free ferrous ions and ROS produced through ferritinophagy. This process serves as the upstream mechanism that triggers ferroptosis, and plays a crucial role in maintaining iron homeostasis and promoting ferroptosis [27–29]. Nuclear receptor coactivator 4 (NCOA4) is a crucial protein for ferritinophagy. It can promotes the autophagic degradation of ferritin and regulate intracellular ferrous iron levels [30–33]. NCOA4 overexpression hyperactivates ferritinophagy, leading to the degradation of ferritin and a concomitant increase in intracellular ferrous iron, ultimately triggering ferroptosis [34]. Conversely, inhibiting inhibiting NCOA4 suppresses ferritin degradation and ferroptosis. Numerous studies have demonstrated that NCOA4-mediated ferritinophagy plays a central role in the progression of various diseases, including ionizing radiation-induced ferroptosis of intestinal epithelial cells, glioblastoma, and triple-negative breast cancer, thereby inducing ferroptosis [35–37]. Related research also indicates that inhibiting ferroptosis can alleviate the inflammatory response in AP accompanied by renal injury and hyperlipidemic pancreatitis [38–40]. Nevertheless, the role of ferroptosis induced by NCOA4-mediated ferritinophagy during the onset of AP remains incompletely understood.

This study aimed to explore the relationship between lactate, lactylation and ferroptosis, as well as the underlying mechanism of high lactate-induced pancreatic injury during the onset of AP. Our results indicated that elevated lactate levels significantly increased H3K18la, and subsequently activated NCOA4-mediated ferroptosis by enhancing NCOA4 transcription, thereby exacerbating tissue injury and inflammation caused by AP. Therefore, we propose that an increase in lactate levels can promote H3K18la, thereby regulating NCOA4-mediated ferroptosis and exacerbating the pancreatic damage caused by AP. These findings offer novel insights into the mechanism of AP.

Materials and Methods

AP Rat Models

Male Sprague-Dawley (SD) rats aged 6–8 weeks were purchased from Jiangsu GemPharmatech Co., Ltd. The animals were randomly assigned to different experimental groups and were fasted for 24 h prior to the experiment. Two intraperitoneal injections of 10% L-arginine (2.5 g/kg, Solarbio, SA8460) were administered at 1 h intervals to establish an in vivo model of AP, as previously described [41]. Rats in the sham group received an equivalent volume of saline. Preliminary experiments indicated that the upward trend in pathological and biochemical indicators observed at 6, 12, and 24 h persisted at 48 h. Consequently, the 48-hour time point was selected as the experimental endpoint for this study. Forty-eight hours after the final intraperitoneal injection, the rats were anesthetized with 1% sodium pentobarbital (50 mg/kg, intraperitoneally). Blood and pancreatic tissues were collected for further analysis. All animal experiments were in accordance with the ARRIVE guidelines and approved by the Ethics Committee of Anhui Medical University (LLSC20200987).

In vivo experiments

To investigate the effects of lactate on AP, rats were intraperitoneally administered sodium lactate (Lac-Na, 2 g/kg, Merck, L7022), sodium oxamate (OXA, an LDH inhibitor, 10 mg/kg, Merck, O2751), or ferrostatin-1 (Fer-1, a ferroptosis inhibitor, 5 mg/kg, GLPBIO, GC10380) respectively 1 h prior to the induction of AP or the sham operation.

Table 1 Primers used for rat genes of qRT- PCR

Name	Sense (5′–3′)	Antisense (5′–3′)
IL-6	ACTTCCAGCCAGTTGCCT TCTTG	TGGTCTGTTGTGG GTGGTATCCTC
TNF-α	TCAAGAGCCCTTGCCCT AAG	TGGAAGACTCCTC CCAGGTA
IL-1β	TGTTTCCCTCCCTGCCTC TGAC	CGACAATGCTGCC TCGTGACC
NCOA4	TGACCGTGACCTGCCAACC	GCCTCAACTCACA GACTTAACTCAG
FTH1	AACCAGCGAGGTGGACG AATC	GCCAGTTTGTGAA GTTCCAGTAGTG
GPX4	ACCAGTTCGGGAGGCAG GAG	CACAGTGGGTGG GCATCGTC
GAPDH	GACATGCCGCCTGGAGA AAC	AGCCCAGGATGC CCTTTAGT

To induce local NCOA4 depletion, AAV9 vectors encoding NCOA4-targeting short hairpin RNA (AAV-sh-NCOA4, General Biol) or control short hairpin RNA (AAV-sh-NC, General Biol) were constructed. Each rat received a tail vein injection of 2 × 10^11 viral genomes. The AP model was considered established after a three-week period of normal feeding.

Hematoxylin–Eosin (HE) Staining

Pancreatic tissues were harvested and fixed in 4% paraformaldehyde (Sangon, E672002) at 4 °C overnight, then embedded in paraffin. Pancreatic tissue sections were stained with hematoxylin–eosin (H&E) and evaluated by two investigators blinded to the experimental groups using light microscopy. Briefly, each H&E-stained section was divided into four quadrants (upper left, lower left, upper right, and lower right), with one random field of view selected per quadrant. According to established pancreatic injury scoring criteria [42], the four histological parameters—edema, necrosis, inflammatory cell infiltration, and hemorrhage—were assessed and scored independently. The edema score, based on progressive expansion at the pancreatic tissue level, is defined as follows: grade 0 indicates no expansion; grade 1 denotes mild expansion of pancreatic tissue (expansion area ≤ 10% in high-power field [HPF]); grade 2 represents moderate expansion of pancreatic tissue (10% < expansion area ≤ 30% in HPF); grade 3 indicates severe expansion of pancreatic tissue (30% < expansion area ≤ 50% in HPF); grade 4 denotes severe expansion of pancreatic tissue (expansion area > 50% in HPF). Necrosis scoring quantifies the distribution and confluence state of necrotic cells in HPF: grade 0 indicates no necrosis; grade 0.5 represents focal presence of 1–4 necrotic cells/HPF; grade 1 denotes diffuse distribution of 1–4 necrotic cells/HPF; grade 1.5 shows diffuse 1–4 necrotic cells accompanied by focal 5–10 necrotic cells/HPF; grade 2 represents diffuse 5–10 necrotic cells/HPF; grade 2.5 adds focal 11–16 necrotic cells/HPF; grade 3 indicates diffuse 11–16 necrotic cells/HPF with confluent necrotic foci formation; grade 3.5 denotes focal presence of > 16 necrotic cells/HPF; grade 4 demonstrates extensive confluent necrosis. Inflammatory infiltration score assesses the number of leukocytes and abscess formation in HPF: grade 0 corresponds to 0–1 leukocytes/HPF; grade 0.5 corresponds to 2–5 leukocytes/HPF; thereafter, the score increases by 0.5 for each approximate increment of 5 leukocytes (grade 1: 6–10; grade 1.5: 11–15; grade 2: 16–20; grade 2.5: 21–25; grade 3: 26–30); grade 3.5 is defined as > 30 leukocytes/HPF or focal microabscesses; grade 4 corresponds to > 35 leukocytes/HPF or confluent microabscesses. Hemorrhage score employs the lesion counting method: grade 0 indicates no lesion; grade 1 represents the presence of a lesion. The scores of these four parameters were summed to generate the histopathological injury score for each quadrant, with higher scores indicating more severe pancreatic tissue damage.

Table 2 Primers used for rat NCOA4 promoter of ChIP-qPCR

Name	Sense (5′–3′)	Antisense (5′–3′)
NCOA4	AACCAGGGTAGAGTC GGGT	TTGCAATCG TAGCATGGG AGA

Table 3 The SiRNA sequences used for rat NCOA4 in this study

Name	Sense (5′–3′)	Antisense (5′–3′)
si-NCOA4	GCUGUUUCUCU	AUUCACUGAGAGAAACAGC
si-NC	CAGUCAAUTT	TT
	UUCUCCGAACG	ACGUGACACGUUCGGAG
	UGUCACGUTT	AATT

Immunofluorescence Staining

Paraffin-embedded tissue sections were cut at a thickness of 5 μm, and then incubated with primary antibodies, including anti-Pan-Kla (PTM, PTM-1401RM), anti-H3K18la (PTM, PTM-1427RM), and anti-Amylase (Proteintech, 66133-1), followed by incubation with appropriate secondary antibodies. Finally, the sections were counterstained with DAPI-containing blocking solution (Biosharp, 23324599) and imaged using an Olympus fluorescence microscope.

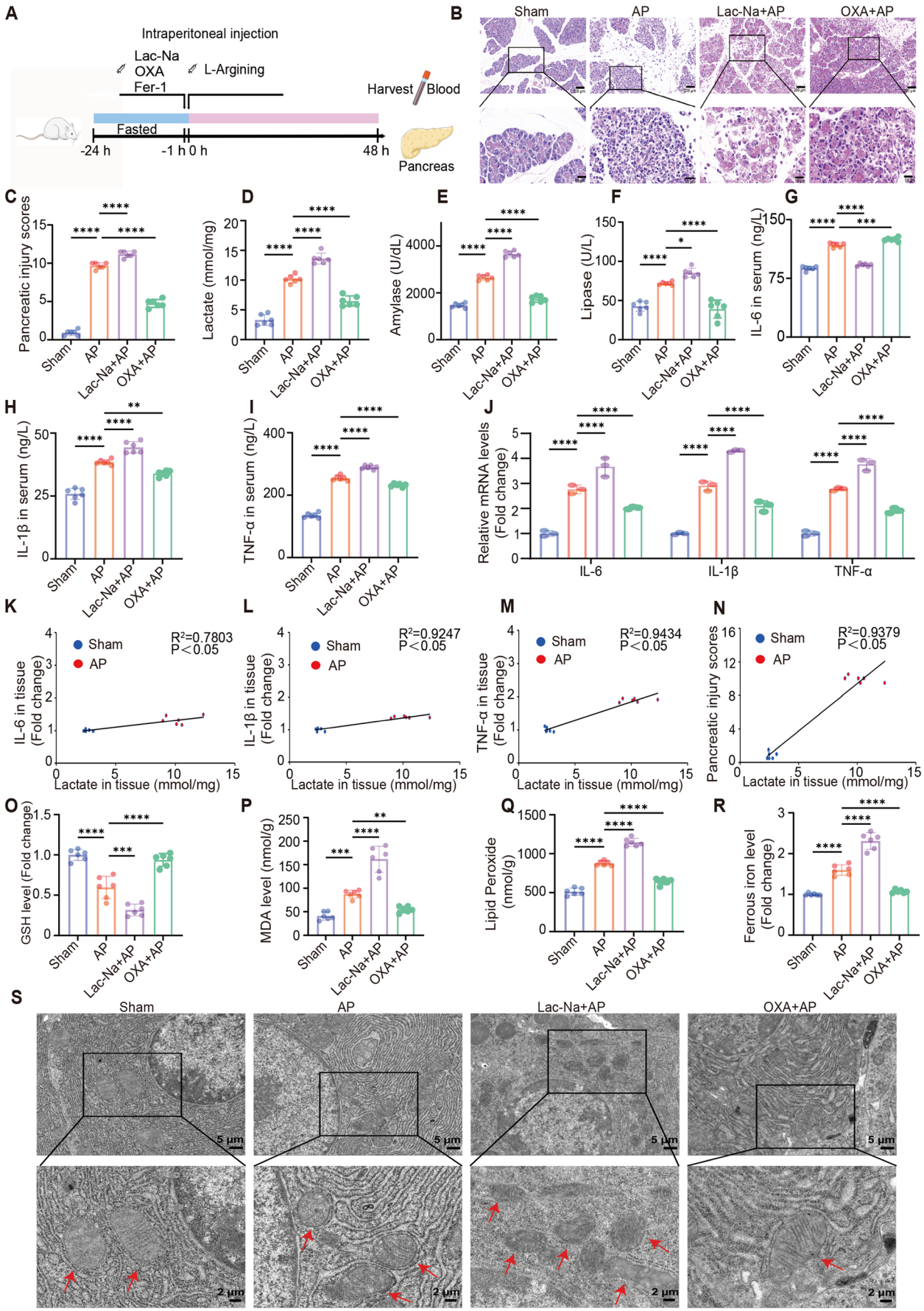

A
Intraperitoneal injection
Lac-Na
OXA
L-Arginine
Fer-1
Harvest Blood
Fasted
-24 h
-1 h 0 h
48 h
Pancreas
B
Sham
AP
Lac-Na+AP
OXA+AP
C
Pancreatic injury scores
D
Lactate (mmol/mg)
E
Amylase (U/dL)
F
Lipase (U/L)
G
IL-6 in serum (ng/L)
H
IL-1β in serum (ng/L)
I
TNF-α in serum (ng/L)
J
Relative mRNA levels (Fold change)
IL-6
IL-1β
TNF-α
K
IL-6 in tissue (Fold change)
R²=0.7803
P<0.05
L
IL-1β in tissue (Fold change)
R²=0.9247
P<0.05
M
TNF-α in tissue (Fold change)
R²=0.9434
P<0.05
N
Pancreatic injury scores
R²=0.9379
P<0.05
Lactate in tissue (mmol/mg)
O
GSH level (Fold change)
P
MDA level (nmol/g)
Q
Lipid Peroxide (nmol/g)
R
Ferrous iron level (Fold change)
S
5 μm
2 μm

Fig. 1 Inhibiting lactate can effectively alleviate pancreatic inflammation, tissue injury and ferroptosis of AP. (**A**) Schematic diagram of AP model rat experimental design. (**B-C**) Representative HE-stained images of pancreatic tissue and corresponding injury scores in Sham, AP, AP with sodium lactate treatment (Lac-Na+AP), and AP with sodium oxamate treatment (OXA+AP) groups ($n=6$ rats per group). (**D**) Pancreatic lactate concentrations in Sham, AP, Lac-Na+AP and OX+AP rats ($n=6$ rats per group). (**E-F**) Serum amylase and lipase levels in Sham, AP, Lac-Na+AP and OXA+AP rats ($n=6$ rats per group). (**G-I**) Serum levels of inflammatory cytokines IL-6, IL-1β, and TNF-α in Sham, AP, Lac-Na+AP, and OXA+AP rats ($n=6$ rats per group). (**J**) mRNA expression levels of IL-6, IL-1β, and TNF-α in pancreatic tissues from Sham, AP, Lac-Na+AP, and OXA+AP rats ($n=6$ rats per group). (**K-N**) Correlations among IL-6, IL-1β, TNF-α mRNA levels, pancreas injury scores and Lactate concentrations ($n=6$ rats per group). (**O-R**) Levels of glutathione (GSH), malondialdehyde (MDA), lipid peroxides, and ferrous iron in pancreatic tissues in Sham, AP, Lac-Na+AP and OXA+AP rats ($n=6$ rats per group). (**S**) Representative TEM images of pancreatic tissue in Sham, AP, Lac-Na+AP and OXA+AP rats. Statistical analyses: One-way ANOVA followed by Tukey'spost hoc test in (C), (D), (E), (F), (G), (H), (I), (O), (P), (Q) and (R); Two-way ANOVA followed by Tukey's post hoc test in (J). Data are presented as mean±SD. *$p<0.05$; **$p<0.01$; ***$p<0.001$; ****$p<0.0001$

Measurement of Lactate Levels

Pancreatic tissue samples were collected and homogenized, followed by centrifugation at 4000 rpm for 20 min. Lactate levels in the supernatant were then quantified using a colorimetric assay kit according to the manufacturer's instructions (Solarbio, BC2230).

Biochemical Indices

Serum levels of interleukin-6 (IL-6, Senbeijia, SBJ-R0755), tumor necrosis factor-alpha (TNF-α, Senbeijia, SBJ-R0040), and interleukin-1 beta (IL-1β, Ruixin Biotech, RX300379R), amylase (Nanjing Jiancheng Bioengineering Institute, C016-1-1), lipase (Nanjing Jiancheng Bioengineering Institute, A054-1-1), pancreatic malondialdehyde (MDA, Sangon, D799761), lipid peroxide (LPO, Sangon, D799602), glutathione (GSH, Abbkine, KTB1600), and Fe^{2+} (Solarbio, BC5415) were quantified using the corresponding commercial kits according to the manufacturers' instructions.

Cell Culture

Rat pancreatic acinar AR42J cells were obtained from American Type Culture Collection (ATCC). AR42J cells were cultured in Ham's F-12 K medium (Biochannel, BC-M-008) supplemented with 100 U/mL penicillin and streptomycin (Sangon, E607011) and 20% fetal bovine serum (FBS, Biochannel, BC-SE-FBS01) at 37 °C in 5% CO_2. The in vitro AP model was established by treating cells with 120 nM caerulein (Solarbio, C6660) for 24 h. All experiments were performed independently in triplicate.

Real-time Quantitative PCR (qRT–PCR)

Total RNA was extracted using TRIzol reagent (Thermo Scientific, 15596026). Complementary DNA (cDNA) was synthesized using HiScript III All-in-One RT SuperMix (Vazyme, R333-01). Gene expression was quantified using SYBR Green real-time quantitative PCR (Vazyme, Q311-02). Gene expression levels were quantified using the $2^{\wedge-\Delta\Delta CT}$ method [43]. The primers used in this study are listed in Table 1.

Western Blot

Protein samples were extracted from pancreatic tissues or AR42J cells using RIPA lysis buffer (Servicebio, G2002) following the manufacturer's instructions. Protein concentrations were measured using a BCA protein assay kit (Beyotime, KTD3001). Equal amounts of protein were separated by SDS-PAGE and transferred onto PVDF membranes (Millipore, ISEQ00010). Membranes were blocked with protein-free rapid blocking buffer (EpiZyme, PS108) for 1 h at room temperature, then incubated overnight at 4 °C with primary antibodies including anti-NCOA4 (Affinity, AF4255), anti-FTH1 (Abcam, ab183781), anti-LC3 (Abcam, ab18709), anti-GPX4 (Affinity, DF6701), Pan-Kla (PTM, PTM-1401RM), anti-H3K14la (PTM, PTM-1414RM), anti-H3K18la (PTM, PTM-1427RM), anti-H4K8la (PTM, PTM-1415RM), and anti-H4K12la (PTM, PTM-1411RM). Subsequently, membranes were incubated with corresponding HRP-conjugated secondary antibodies (anti-GAPDH, Protientech, 60004-1) for 1 h at room temperature. Protein bands were detected using enhanced chemiluminescence reagent (Proteintech, PK1000). Protein bands were quantified using ImageJ software. The intensity of each target protein was normalized to that of the corresponding loading control (H3 or GAPDH).

Transmission Electron Microscopy (TEM)

Pancreatic tissue from rats was dissected into 1 mm^3 pieces and subsequently fixed in 4% glutaraldehyde (Servicebio, G1102). The samples were then processed further by staining with 1% uranyl acetate and 0.2% lead citrate. Finally, the prepared specimens were examined using a HITACHI HT7800 transmission electron microscope.

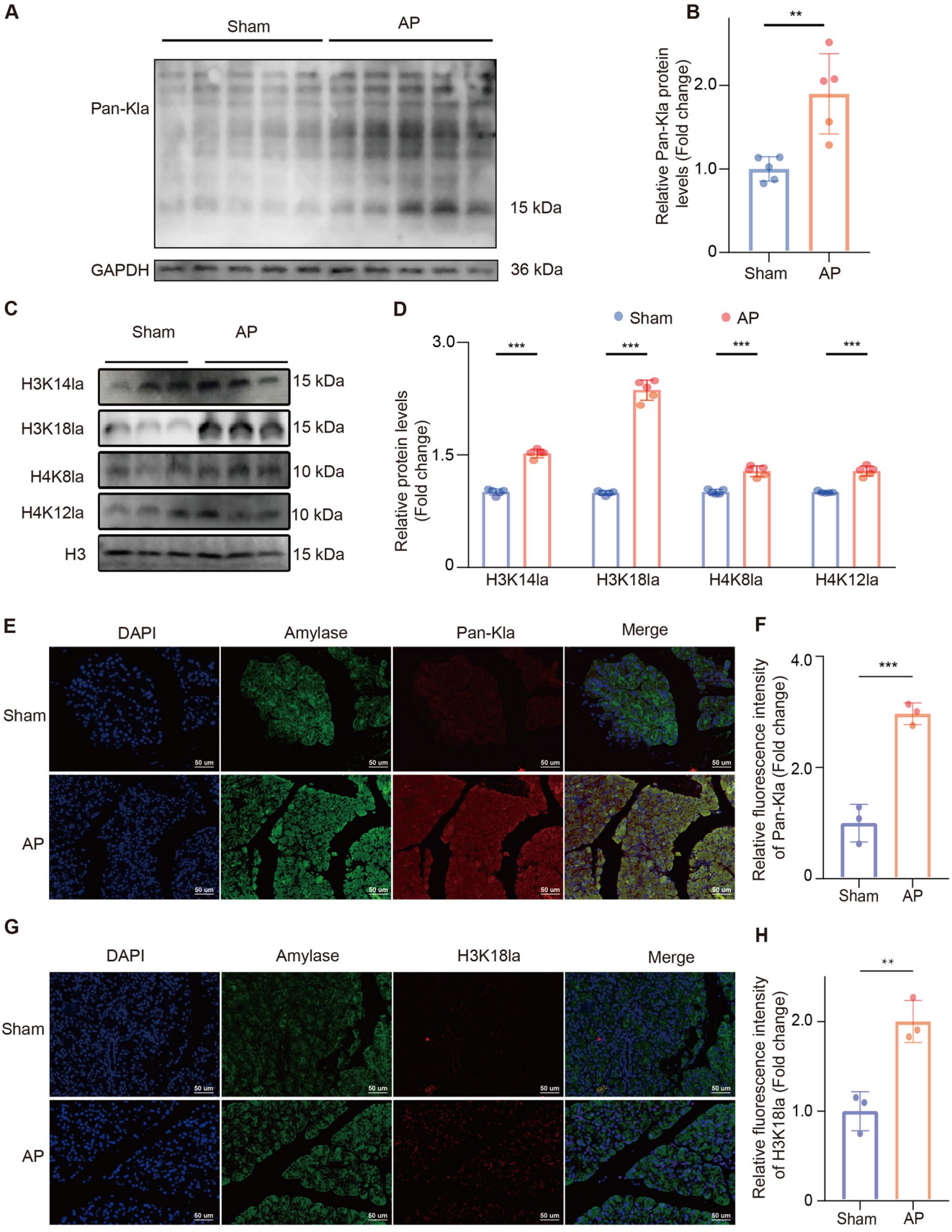

A
Sham
AP
Pan-Kla
15 kDa
GAPDH
36 kDa
B
**
Relative Pan-Kla protein levels (Fold change)
2.0
1.0
0
Sham
AP
C
Sham
AP
H3K14la
15 kDa
H3K18la
15 kDa
H4K8la
10 kDa
H4K12la
10 kDa
H3
15 kDa
D
Sham
AP
***
Relative protein levels (Fold change)
3.0
1.5
0
H3K14la
H3K18la
H4K8la
H4K12la
E
DAPI
Amylase
Pan-Kla
Merge
Sham
AP
50 um
F
***
Relative fluorescence intensity of Pan-Kla (Fold change)
4.0
2.0
0
Sham
AP
G
DAPI
Amylase
H3K18la
Merge
Sham
AP
50 um
H
**
Relative fluorescence intensity of H3K18la (Fold change)
2.0
1.0
0
Sham
AP

Fig. 2 Lactate enhances histone- lysines lactylation in AP. (**A**-**B**) Western blot images and relative protein levels of Pan-Kla in pancreatic tissues from Sham and AP rats ($n=5$ rats per group). (**C**-**D**) Western blot images and relative protein levels of histone lactylation (H3K14la, H3K18la, H4K8la, H4K12la) in pancreatic tissues from Sham and AP rats ($n=5$ rats per group). (**E**-**F**) Representative immunofluorescence images and relative fluorescence intensity of Pan-Kla co-localized with amylase in pancreatic tissues from Sham and AP rats. (**G**-**H**) Representative immunofluorescence images and relative fluorescence intensity of H3K18la co-localized with amylase in pancreatic tissues from Sham and AP rats. Statistical analyses: Student's t-test in (B), (F), and (H); Two-way ANOVA followed by Tukey's post hoc test in (D). Data are presented as mean ± SD. *$p<0.05$; **$p<0.01$; ***$p<0.001$; ****$p<0.0001$

FeRhNOX-1 Assay

Intracellular ferrous iron levels in AR42J cells were quantified using the FeRhoNox-1 kit (MKbio, MX4558) following the manufacturer's protocols. Subsequently, the cells were visualized by laser scanning confocal microscopy.

Analysis of Reactive Oxygen Species (ROS)

Intracellular reactive oxygen species (ROS) levels in AR42J cells were measured using the CM-H2DCFH-DA kit (Beyotime, S0033S) following the manufacturer's protocol. The cells were subsequently observed and analyzed using laser scanning confocal microscopy.

Mitochondrial Membrane Potential (MMP)

Changes in mitochondrial membrane potential (MMP) were measured using the JC-1 MMP assay kit (Abbkine, KTA4001) according to the manufacturer's instructions. Cells were imaged using a fluorescence microscope. Red fluorescent aggregates represent mitochondria with intact membrane potential, while green fluorescent monomers indicate a decrease in MMP [23].

Cleavage Under Targets and Tagmentation (CUT&Tag)

CUT&Tag library amplification and purification were conducted using the Hyperactive In Situ Chromatin Immunoprecipitation (ChIP) Library Prep Kit for Illumina (Vazyme, TD904-01) following the manufacturer's instructions. Briefly, concanavalin A-coated beads were employed to capture the pancreatic tissue sample of AP. After resuspending in antibody buffer, the samples were subjected to sequential incubation with anti-H3K18la primary antibody (PTM, PTM-1427RM) and anti-rabbit IgG H&L secondary antibody (Abbkine, A21030). Subsequently, the samples were incubated with pA-Tn5 transposase. After the transposase activation and tagmentation, the fragment DNA was isolated, amplified and purified, and the library was established. The sequencing library was further purified using NovoNGS DNA Clean Beads. DNA libraries were sequenced on the Illumina platform, and raw sequence data were processed by Tsingke Biotech. Peak visualization was performed using IGV v2.14.1.

RNA Sequencing (RNA-seq)

Total RNA was extracted from the rat pancreatic tissue for RNA-seq analysis using the Illumina 10 platform. Differentially expressed genes between the two groups were identified based on log2-fold change (log2FC) values, with a significance cutoff of $P<0.05$. The results were visualized as heatmaps to facilitate functional analysis.

ChIP-qPCR

AR42J cells were treated with 10 mM Lac-Na or PBS for 24 h. After treatment, cells were washed three times with PBS and cross-linked in 9 mL of medium containing 1% formaldehyde, with the reaction quenched by adding 125 mM glycine (Sangon, A422274). Chromatin was extracted using a High Sensitivity ChIP Kit (Beyotime, ELS-ENZ-GEN509-0012) following the manufacturer's instructions. Chromatin immunoprecipitation (ChIP) was carried out with 2 µg of chromatin and an anti-H3K18la antibody (PTM, PTM-1427RM). After reversing the cross-links and purifying DNA, qPCR was performed using 1 µL of eluted DNA and primers targeting specific regions (Table 2).

SiRNA Transfection

NCOA4 siRNA (si-NCOA4) and negative control siRNA (si-NC) were synthesized by Sangon. The detailed sequences of the siRNAs targeting the nucleotides of 648–667 in rat NCOA4 mRNA (NM_001034007.1) are listed in Table 3. Transfection was carried out using Lipofectamine™ 2000.

Statistical Analysis

Data were analyzed using GraphPad Prism software (version 9.0) and are expressed as mean ± standard deviations from at least three independent experiments. Student's t-test was applied for comparisons between two groups, and one-way or two-way analysis of variance (ANOVA) followed by Tukey's post hoc test was used for comparisons between multiple groups. P value <0.05 was considered statistically significant.

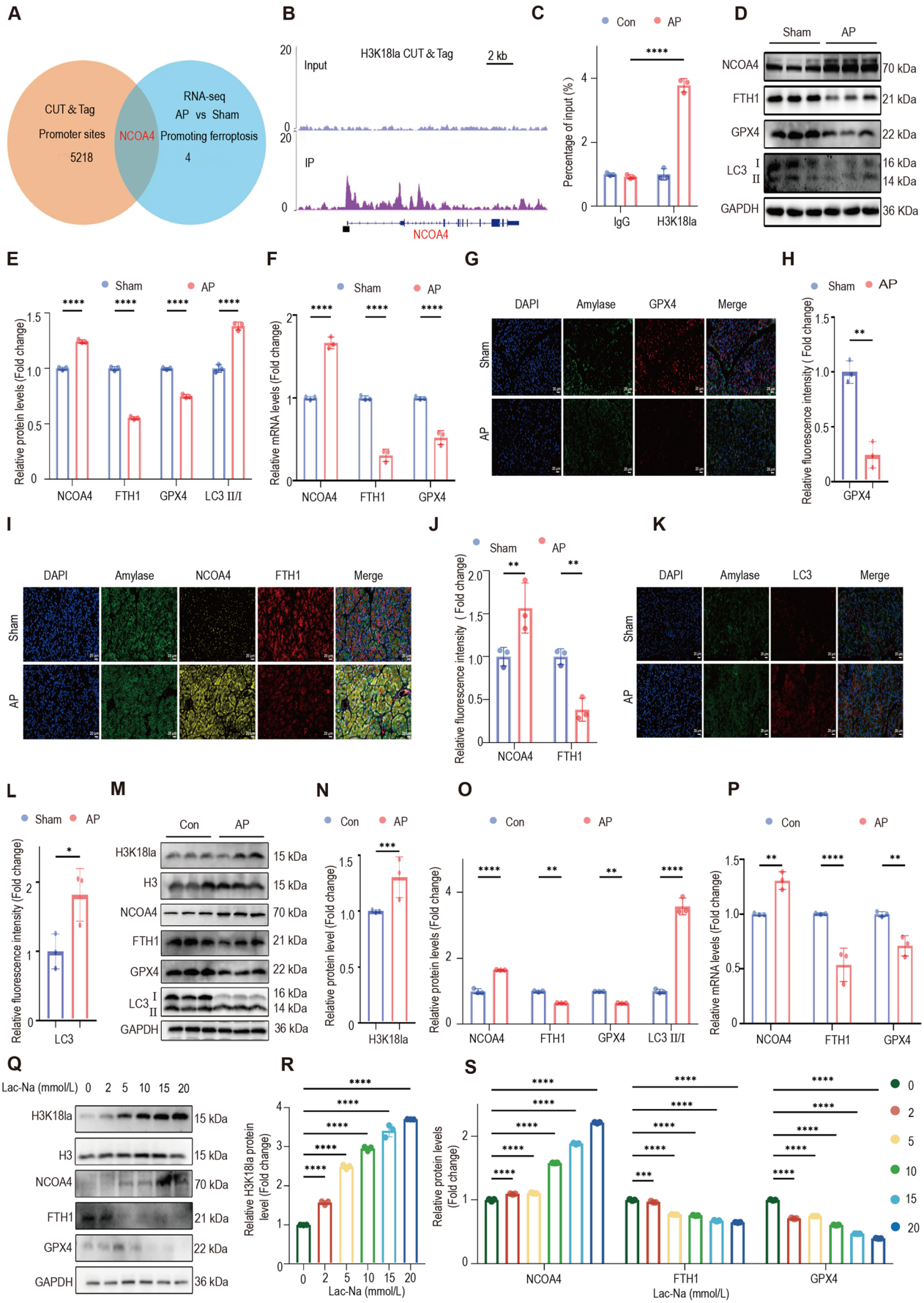

A
CUT & Tag
Promoter sites
5218
NCOA4
RNA-seq
AP vs Sham
Promoting ferroptosis
4
B
H3K18la CUT & Tag
Input
IP
2 kb
NCOA4
C
Con
AP
Percentage of input (%)
IgG
H3K18la
D
Sham
AP
NCOA4
FTH1
GPX4
LC3 I
II
GAPDH
70 kDa
21 kDa
22 kDa
16 kDa
14 kDa
36 kDa
E
Relative protein levels (Fold change)
NCOA4
FTH1
GPX4
LC3 II/I
F
Relative mRNA levels (Fold change)
G
DAPI
Amylase
GPX4
Merge
H
Relative fluorescence intensity (Fold change)
I
DAPI
Amylase
NCOA4
FTH1
Merge
J
Relative fluorescence intensity (Fold change)
K
DAPI
Amylase
LC3
Merge
L
Relative fluorescence intensity (Fold change)
M
H3K18la
H3
15 kDa
Relative protein level (Fold change)
N
O
Relative protein levels (Fold change)
P
Relative mRNA levels (Fold change)
Q
Lac-Na (mmol/L) 0 2 5 10 15 20
R
Relative H3K18la protein level (Fold change)
Lac-Na (mmol/L)
S
Relative protein levels (Fold change)
Lac-Na (mmol/L)

Fig. 3 H3K18 lactylation (H3K18la) activates NCOA4 transcription in AP. (**A**) Overlapping ferroptosis-related genes identified by CUT&Tag and RNA-seq analyses ($n=3$ rats per group). (**B**) IGV tracks showing NCOA4 from CUT&Tag analysis using H3K18la antibodies in pancreatic tissue of AP rats. (**C**) ChIP-qPCR analysis of H3K18la enrichment at the NCOA4 promoter in AR42J cells treated with sodium lactate (Lac-Na) or PBS (control) ($n=3$ biologically independent samples per group). (**D-E**) Western blot images and relative protein levels of NCOA4, FTH1, GPX4 and LC3 in pancreatic tissues from Sham and AP rats. (**F**) NCOA4, FTH1 and GPX4 mRNA expression levels of pancreas tissues in Sham and AP rats. (**G-L**) Representative immunofluorescence images and relative fluorescence intensity of GPX4, NCOA4 and FTH1, LC3 co-localized with amylase in pancreatic tissues from Sham and AP rats. (**M-O**) Western blot images and relative protein levels of H3K18la, NCOA4, FTH1, GPX4 and LC3 protein level in AR42J cells treated with PBS (Con) and caerulein (AP) ($n=3$ biologically independent samples per group). (**P**) NCOA4, FTH1 and GPX4 mRNA expression levels of AR42J cells treated with PBS (Con) and caerulein (AP) ($n=3$ biologically independent samples per group). (**Q-S**) Western blot images and relative protein levels of H3K18la, NCOA4, FTH1 and GPX4 in AR42J cells stimulated with varying concentrations of sodium lactate (Lac-Na) ($n=3$ biologically independent samples per group). Statistical analyses: Student's t-test in (H), (L), and (N); One-way ANOVA followed by Tukey's post hoc test in (R); Two-way ANOVA followed by Tukey's post hoc test in (C), (E), (F), (J), (O), (P) and (S). Data are presented as mean ± SD. *$p<0.05$; **$p<0.01$; ***$p<0.001$; ****$p<0.0001$

Results

Inhibiting Lactate Production Effectively Alleviates Pancreatic inflammation, Tissue Injury and Ferroptosis of AP

To investigate the role of lactate in AP, rat models were established to mimic clinical conditions (Fig. 1A). Sodium lactate (Lac-Na) and Oxamate (OXA) were administered to enhance exogenous lactate and inhibit endogenous lactate production. As reported previously, OXA acts as an effective inhibitor of lactate dehydrogenase (LDH) by competing with pyruvate for the binding site on the LDH [18, 23]. One hour prior to AP induction by L-Arginine, Lac-Na (Lac-Na + AP group) and OXA (OXA + AP group) were administered. In the pancreas of rats with AP, showed obvious interstitial edema, necrosis, inflammatory cell infiltration and hemorrhage (Fig. 1B and Figure S1). Moreover, the pancreatic injury score (Fig. 1C), lactate levels in pancreas and serum (Fig. 1D and Figure S2A), serum amylase (Fig. 1E), lipase (Fig. 1F), and inflammatory cytokines (Fig. 1G-I) in the AP group significantly increased, confirming that the establishment of the AP rat model was successful. Compared with the AP group, Lac-Na pretreatment aggravated pancreatic injury, whereas OXA pretreatment alleviated the pancreatic injury caused by AP (Fig. 1B-C, Figure S1). The lactate levels in both pancreatic tissues and serum of AP group rats were both significantly higher than those of the sham group (Fig. 1D and Figure S2A). Lac-Na pretreatment further elevated the concentrations of amylase (Fig. 1E), lipase (Fig. 1F), and inflammatory cytokines in serum (Fig. 1G-I), as well as the mRNA expression levels of inflammatory cytokines in pancreatic tissue (Fig. 1J). In contrast, OXA pretreatment exhibited a protective effect on AP by inhibiting pancreatic damage, amylase, lipase, and inflammation (Fig. 1D, Figure S2A and Fig. 1E-J). Correlation analysis showed positive associations between lactate levels and inflammatory cytokines as well as pancreatic injury (Fig. 1K-N, Figure S2B-D). Compared with the Sham group, GSH levels in the AP group were decreased, while the levels of malondialdehyde (MDA), lipid peroxidation, and ferrous iron were higher (Fig. 1O-R). Transmission electron microscopy (TEM) observations revealed that compared with Sham group, AP rats exhibited typical mitochondrial morphology of ferroptosis, including mitochondrial shrinkage, outer membrane rupture, and reduction of cristae (Fig. 1S). Compared with the AP group, the GSH level in the Lac-Na + AP group was decreased, while the levels of MDA, lipid peroxide, and ferrous iron were elevated (Fig. 1O-R). The AP-induced mitochondrial damage was exacerbated in Lac-Na + AP group (Fig. 1S). Compared with the AP group, GSH level in OXA + AP group increased, while lipid peroxide, MDA, and ferrous iron levels were reduced (Fig. 1O-R). The mitochondrial morphology in OXA + AP group was restored (Fig. 1S). These findings suggest that an increase in lactate might exacerbate the inflammatory response, pancreatic injury and ferroptosis in AP. Lactate inhibition significantly alleviated inflammation, pancreatic injury, and ferroptosis in AP.

Lactate Promotes an Obvious Increase in H3K18 Lactylation (H3K18la) in AP

To elucidate the precise role of lactate-derived lactylation in the pathogenesis of AP, we measured pan-lysine lactylation (Pan-Kla) levels in the pancreas of rats from the Sham and AP groups. Compared with the Sham group, Pan-Kla levels were significantly elevated in the AP group was significantly increased, and histone lactylation showing particularly notable increases (Fig. 2A and 2B). Various lysine lactylation sites on histones were subsequently identified, including H3K14 (H3K14la), H3K18 (H3K18la), H4K8 (H4K8la), and H4K12 (H4K12la). H3K18la levels were significantly higher in AP rats compared to Sham rats (Fig. 2C-D). Immunofluorescence co-staining with anti-amylase (a marker of pancreatic acinar cells) confirmed substantial increases in both Pan-Kla and H3K18la levels within pancreatic acinar cells (Fig. 2E-H). These findings suggest that lactate enhances H3K18la levels in pancreatic acinar cells during AP onset.

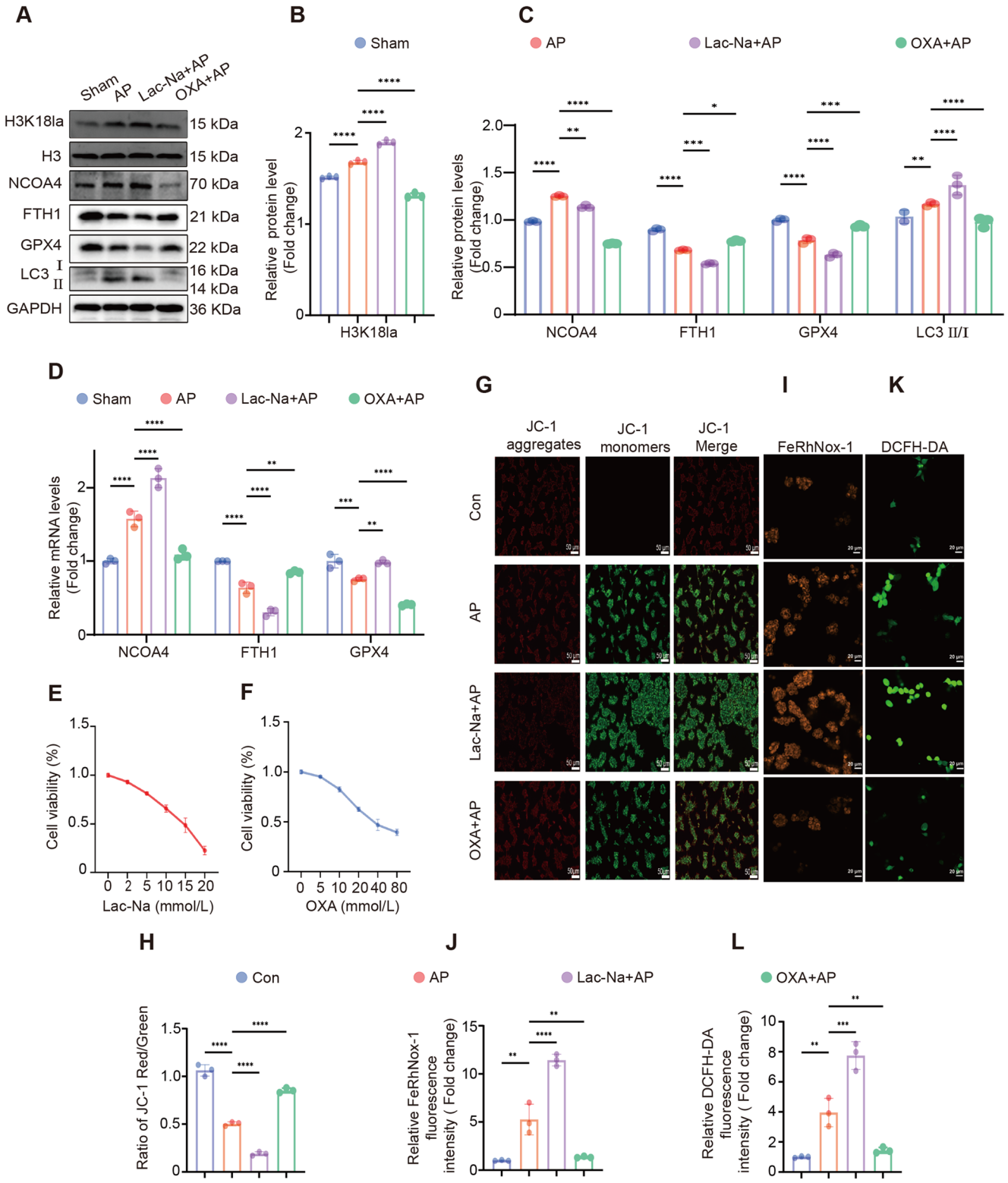

A
Sham
AP
Lac-Na+AP
OXA+AP
H3K18la
H3
NCOA4
FTH1
GPX4
LC3 I
LC3 II
GAPDH
15 kDa
15 kDa
70 kDa
21 kDa
22 kDa
16 kDa
14 kDa
36 KDa
B
Sham
Relative protein level (Fold change)
H3K18la
C
AP
Lac-Na+AP
OXA+AP
Relative protein levels (Fold change)
NCOA4
FTH1
GPX4
LC3 II/I
D
Sham
AP
Lac-Na+AP
OXA+AP
Relative mRNA levels (Fold change)
NCOA4
FTH1
GPX4
E
Cell viability (%)
Lac-Na (mmol/L)
F
Cell viability (%)
OXA (mmol/L)
G
JC-1 aggregates
JC-1 monomers
JC-1 Merge
Con
AP
Lac-Na+AP
OXA+AP
I
FeRhNox-1
K
DCFH-DA
H
Con
Ratio of JC-1 Red/Green
J
AP
Lac-Na+AP
Relative FeRhNox-1 fluorescence intensity (Fold change)
L
OXA+AP
Relative DCFH-DA fluorescence intensity (Fold change)

Fig. 4 Inhibiting lactate can effectively suppress NCOA4-mediated ferroptosis during the onset of AP. (**A**, **B** and **C**) Western blot images and relative protein levels of H3K18la, NCOA4, FTH1, GPX4 and LC3 in pancreatic tissues from Sham, AP, Lac-Na+AP and OXA+AP rats ($n=3$ rats per group). (**D**) NCOA4, FTH1 and GPX4 mRNA expression levels of pancreas tissues in Sham, AP, Lac-Na+AP and OXA+AP rats. (**E** and **F**) Cell viability of AR42J cells treated with varying concentrations of sodium lactate (Lac-Na) and oxamate (OXA) ($n=3$ biologically independent samples per group). (**G-L**) Representative images and quantification of JC-1, FeRhNOX-1 and DCFH-DA in AR42J cells treated with PBS (Con), caerulein (AP), Lac-Na+caerulein (Lac-Na+AP) and OXA+caerulein (OXA+AP) ($n=3$ biologically independent samples per group). Statistical analyses: One-way ANOVA followed by Tukey's post hoc test in (B), (H), (J) and (L); Two-way ANOVA followed by Tukey's post hoc test in (C) and (D). Data are presented as mean±SD. *$p<0.05$; **$p<0.01$; ***$p<0.001$; ****$p<0.0001$

H3K18 Lactylation Induced by Lactate Activates NCOA4 in AP

Based on our aforementioned findings and previous studies [23], we hypothesized that elevated lactate levels lead to increased H3K18la, thereby promoting ferroptosis in pancreatic acinar cells and exacerbating pancreatic injury in AP. To investigate this, CUT&Tag analysis was performed using anti-H3K18la antibodies, coupled with RNA-seq analysis. Enriched promoter regions identified by CUT&Tag were overlapped with ferroptosis-related genes differentially expressed in RNA-seq. Among these, NCOA4, a ferroptosis enhancer gene, was identified (Fig. 3A). NCOA4 showed significant enrichment of H3K18la peaks at its promoter region (Fig. 3B). which was further confirmed by ChIP-qPCR assays (Fig. 3C). In addition, dual luciferase reporter assays demonstrated that NCOA4 promoter activity was enhanced by Lac-Na but suppressed by si-EP300 and oxamate treatment (Figure S3).

To validate RNA-seq results, the expression levels of NCOA4-mediated ferroptosis-related genes were detected. Compared to the Sham group, protein levels of NCOA4 and LC3 II/I protein levels were significantly elevated, while FTH1 and GPX4 protein levels were markedly lower in AP group (Fig. 3D and 3E). qRT-PCR results showed consistent trends (Fig. 3F). Immunofluorescence co-staining with anti-amylase confirmed these observations, indicating that NCOA4-mediated ferroptosis occurred in pancreatic acinar cells during AP onset (Fig. 3G-L). Additionally, the rat pancreatic acinar cell line AR42J was treated with caerulein to establish an AP model *in vitro*. Western blot and qRT-PCR results in AR42J cells were consistent with those observed in the in vivo rat AP model (Fig. 3M-P). Furthermore, with increasing lactate levels, expressions of H3K18la and NCOA4 increased, while FTH1 and GPX4 expressions decreased in AR42J cells (Fig. 3Q-S). These findings suggested that during the onset of AP, elevated lactate promoted an increase in H3K18la levels, thereby enhancing NCOA4 transcription in pancreatic acinar cells.

Inhibiting Lactate Can Effectively Suppress NCOA4-mediated Ferroptosis during the Onset of AP

Next, we further investigated the regulatory relationship among lactate, H3K18la and NCOA4-mediated ferroptosis. Compared with AP rats, rats treated with Lac-Na+AP exhibited increased expression of H3K18la, NCOA4, and LC3 II/I, alongside decreased levels of FTH1 and GPX4 (Fig. 4A-D, Figure S4). Conversely, OXA+AP group showed reduced H3K18la, NCOA4 and LC3II/I expressions, enhanced FTH1 and GPX4 expressions (Fig. 4A-D). As illustrated in Fig. 3Q-R, treatment with 10 mM Lac-Na significantly upregulated H3K18la expression, with cell viability exceeding 65% (Fig. 4E). Additionally, the data in Figure S5 demonstrated that 20 mM OXA markedly inhibited H3K18la expression, while maintaining cell viability above 65% (Fig. 4F). Therefore, 10 mM Lac-Na and 20 mM OXA were selected for further in vitro experiments. In the AP model in vitro, mitochondrial membrane potential (MMP) was decreased (Fig. 4G and H), whereas ferrous iron and ROS levels were elevated (Fig. 4I-L). Pretreatment with 10 mM Lac-Na (Lac-Na+AP) further increased intracellular ferrous iron and ROS levels and decreased MMP (Fig. 4G-L). In contrast, 20 mM OXA pretreatment reduced intracellular ferrous iron and ROS levels and restored MMP to normal levels (Fig. 4G-L). Collectively, these results suggest that lactate promoted NCOA4-mediated ferroptosis, whereas the inhibition of lactate production attenuates this process.

Inhibition of Ferroptosis Rescues the Adverse Effect of NCOA4-mediated Ferroptosis in AP

In validate the effect of autophagy on ferroptosis in AP, the autophagy inhibitor 3-MA was applied to AR42J cells in vitro. As shown in Figure S6, 3-MA treatment suppressed the expression of NCOA4 and LC3 II/I, while upregulating FTH1 and GPX4. Furthermore, intracellular ferrous iron and ROS levels were decreased following 3-MA administration, indicating that autophagy contributes to the induction of ferroptosis in the AP model (Figure S6). Ferrostatin-1 (Fer-1), a known ferroptosis inhibitor, exerts its effect by enhancing GPX4 expression [44]. To further investigate the role of NCOA4-mediated ferroptosis in AP progression, Fer-1 was administered. Compared with

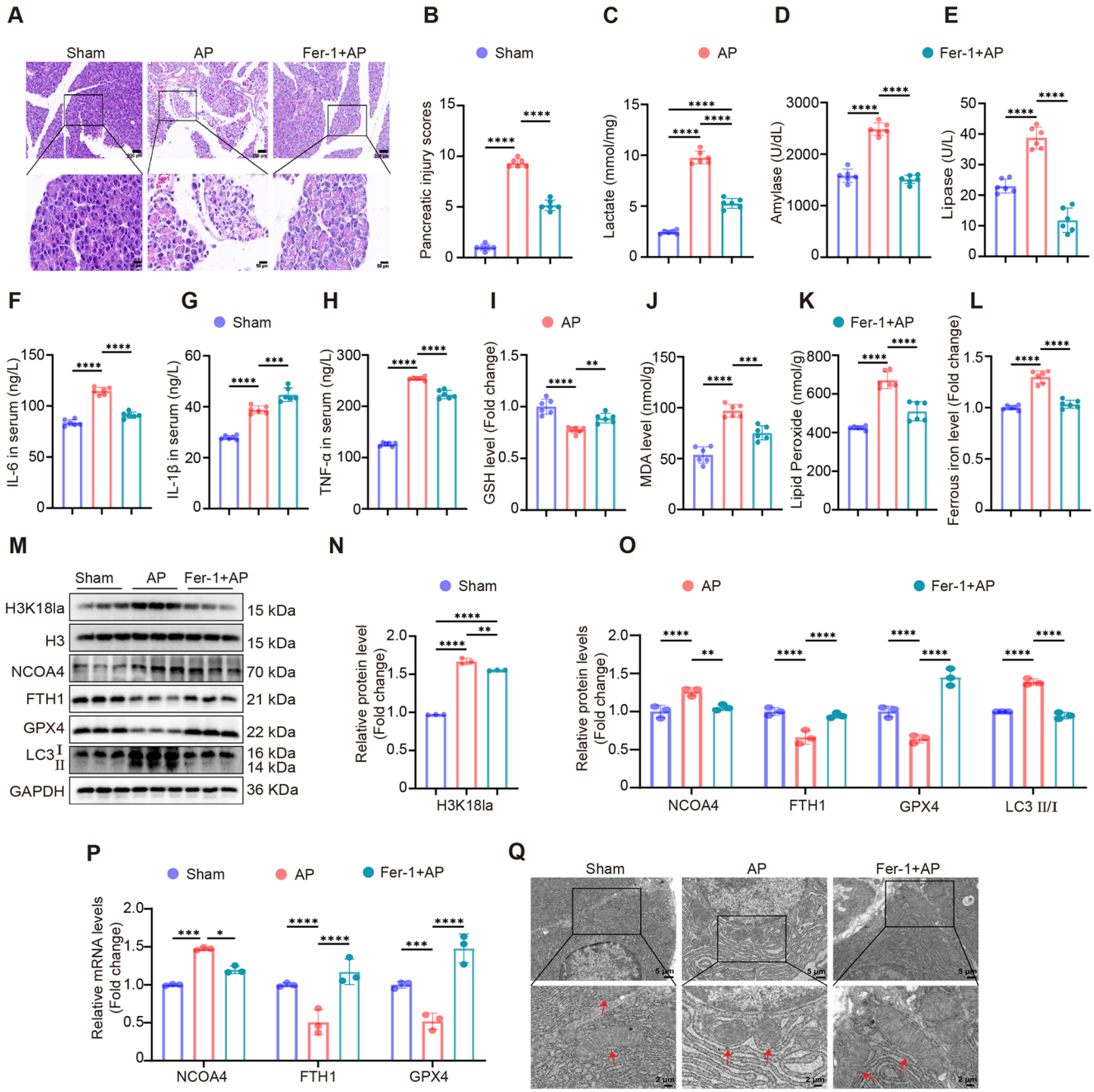


Fig. 5 Inhibition of ferroptosis rescues the adverse effect of NCOA4-mediated ferroptosis of AP rats *in vivo* (**A**,**B**) Representative HE-stained images and injury score of pancreatic injury scores in Sham, AP, AP rats treated with Fer-1 (Fer-1 + AP) (n=6 rats per group). (**C**) Pancreatic lactate concentrations of rats in Sham, AP, and Fer-1 + AP rats (n=6 rats per group). (**D**,**E**) Serum amylase and lipase levels of Sham, AP, and Fer-1 + AP rats (n=6 rats per group). (**F**-**H**) Serum levels of inflammatory cytokines IL-6, IL-1β, and TNF-α of Sham, AP, and Fer-1 + AP rats (n=6 rats per group). (**I**-**L**) Levels of glutathione (GSH), malondialdehyde (MDA), lipid peroxides, and ferrous iron in pancreatic tissues in Sham, AP, and Fer-1 + AP rats (n=6 rats per group). (**M**-**O**) Protein levels of H3K18la, NCOA4, FTH1, GPX4, and LC3 in pancreatic tissues in Sham, AP, and Fer-1 + AP rats. (**P**) mRNA expression levels of NCOA4, FTH1, and GPX4 in pancreatic tissues in Sham, AP, and Fer-1 + AP rats. (**Q**) Representative TEM images of pancreas in Sham, AP, and Fer-1 + AP rats. Statistical analyses: One-way ANOVA followed by Tukey's post hoc test in (B), (C), (D), (E), (F), (G), (H), (I), (J), (K), (L) and (N); Two-way ANOVA followed by Tukey's post hoc test in (O) and (P). Data are presented as mean ± SD. *$p< 0.05$; **$p < 0.01$; ***$p< 0.001$; ****$p< 0.0001$

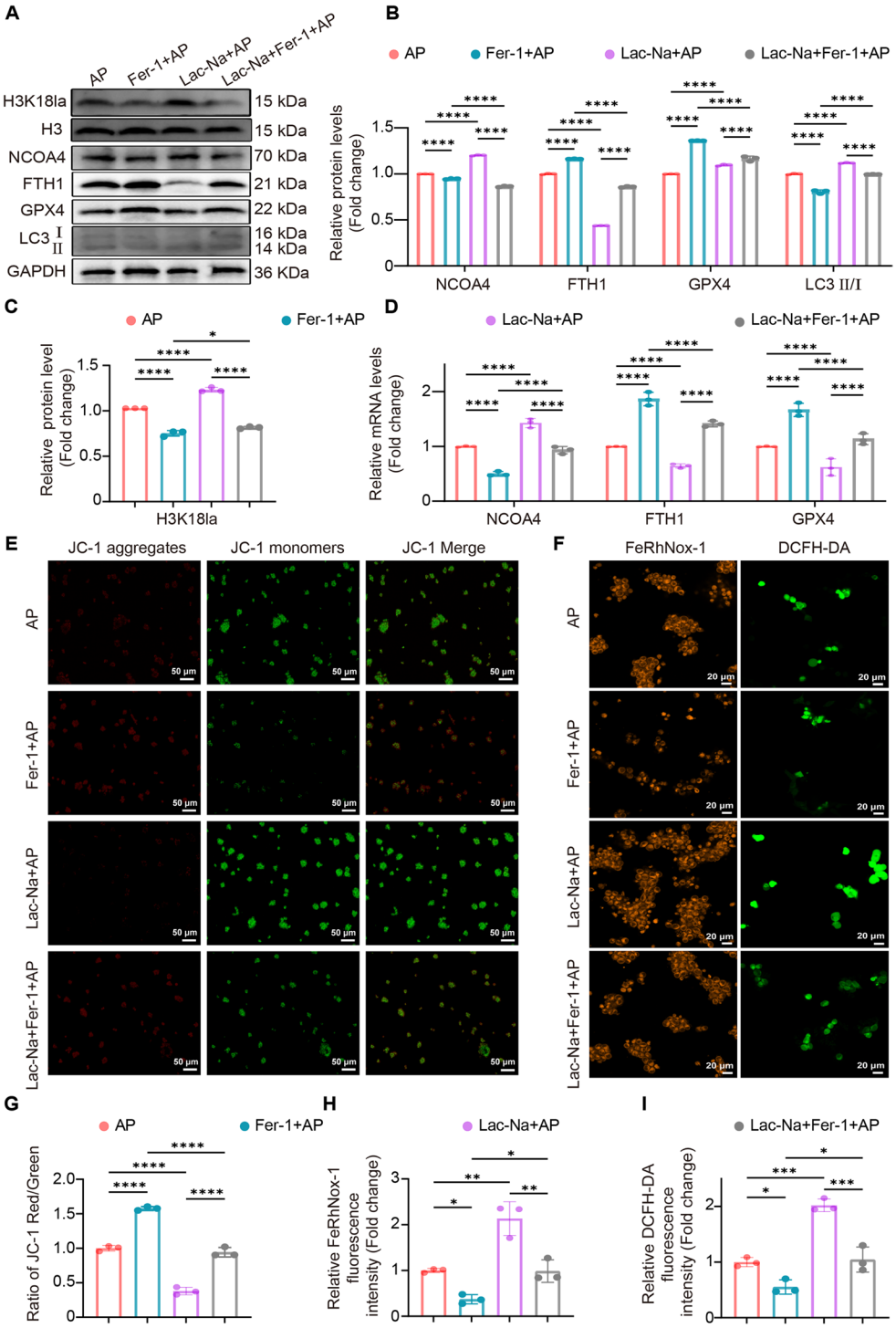


Fig. 6 Inhibition of ferroptosis rescues the adverse effect of NCOA4-mediated ferroptosis of AP (**A**-**C**) Protein levels of H3K18la, NCOA4, FTH1, GPX4, and LC3 in AR42J cells treated with caerulein (AP), Fer-1 + caerulein (Fer-1 + AP), sodium lactate + caerulein (Lac-Na + AP), and sodium lactate + Fer-1 + caerulein (Lac-Na + Fer-1 + AP) (n=3 biologically independent samples per group). (**D**) mRNA expression levels of NCOA4, FTH1, and GPX4 in AR42J cells treated with AP, Fer-1 + AP, Lac-Na + AP and Lac-Na + Fer-1 + AP (n=3 biologically independent samples per group). (**E**-**I**) Representative images and quantification of JC-1, FeRhNOX-1, and DCFH-DA fluorescence in AR42J cells treated with AP, Fer-1+ AP, Lac-Na+ AP and Lac-Na+ Fer-1+ AP (n=3 biologically independent samples per group). Statistical analyses: Two-way ANOVA followed by Tukey's post hoc test in (B) and (D); One-way ANOVA followed by Tukey's post hoc test in (C), (G), (H) and (I). Data are presented as mean ± SD. *p< 0.05; **p< 0.01; ***p< 0.001; ****p< 0.0001

the AP group, Fer-1 pretreatment (Fer-1 + AP group) significantly alleviated pancreatic tissue damage (Fig. 5A-B), reduced pancreatic lactate (Fig. 5C), serum amylase (Fig. 5D), lipase (Fig. 5E), and inflammatory cytokines (Fig. 5F-H), elevated GSH levels (Fig. 5I), and lowered MDA, lipid peroxide, and ferrous iron levels (Fig. 5J-L). In addition, Fer-1 pretreatment decreased the expression of H3K18la, NCOA4, and LC3 II/I, while increasing FTH1 and GPX4 expression (Fig. 5M-P). TEM observations further revealed that Fer-1 pretreatment ameliorated

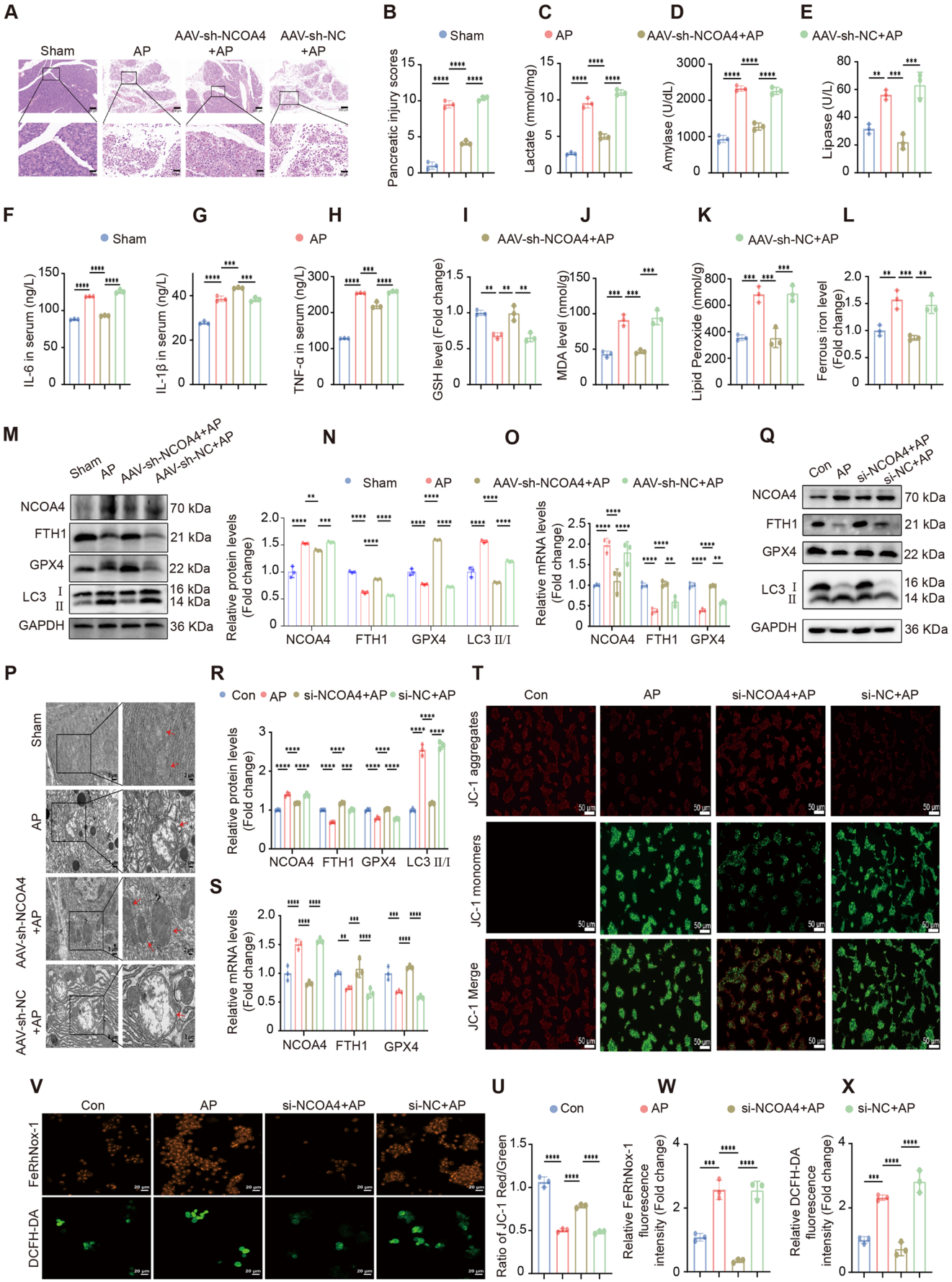

A
Sham
AP
AAV-sh-NCOA4 +AP
AAV-sh-NC +AP
B
Sham
Pancreatic injury scores
C
AP
Lactate (mmol/mg)
D
AAV-sh-NCOA4+AP
Amylase (U/dL)
E
AAV-sh-NC+AP
Lipase (U/L)
F
Sham
IL-6 in serum (ng/L)
G
IL-1β in serum (ng/L)
H
AP
TNF-α in serum (ng/L)
I
AAV-sh-NCOA4+AP
GSH level (Fold change)
J
MDA level (nmol/g)
K
AAV-sh-NC+AP
Lipid Peroxide (nmol/g)
L
Ferrous iron level (Fold change)
M
Sham
AP
AAV-sh-NCOA4+AP
AAV-sh-NC+AP
NCOA4
FTH1
GPX4
LC3 I II
GAPDH
70 kDa
21 kDa
22 kDa
16 kDa
14 kDa
36 KDa
N
Sham
AP
AAV-sh-NCOA4+AP
AAV-sh-NC+AP
Relative protein levels (Fold change)
NCOA4
FTH1
GPX4
LC3 II/I
O
Relative mRNA levels (Fold change)
NCOA4
FTH1
GPX4
Q
Con
AP
si-NCOA4+AP
si-NC+AP
NCOA4
FTH1
GPX4
LC3 I II
GAPDH
70 kDa
21 kDa
22 kDa
16 kDa
14 kDa
36 KDa
P
Sham
AP
AAV-sh-NCOA4 +AP
AAV-sh-NC +AP
R
Con
AP
si-NCOA4+AP
si-NC+AP
Relative protein levels (Fold change)
NCOA4
FTH1
GPX4
LC3 II/I
S
Relative mRNA levels (Fold change)
NCOA4
FTH1
GPX4
T
Con
AP
si-NCOA4+AP
si-NC+AP
JC-1 aggregates
JC-1 monomers
JC-1 Merge
50 μm
V
Con
AP
si-NCOA4+AP
si-NC+AP
FeRhNox-1
DCFH-DA
20 μm
U
Con
Ratio of JC-1 Red/Green
W
AP
si-NCOA4+AP
Relative FeRhNox-1 fluorescence intensity (Fold change)
X
si-NC+AP
Relative DCFH-DA fluorescence intensity (Fold change)

Fig. 7 NCOA4 suppression inhibits ferroptosis and ameliorates AP (**A**–**B**) Representative HE-stained images and injury scores of pancreatic injury scores tissues in Sham, AP, AAV-sh-NCOA4+ AP and AAV-sh-NC+ AP rats (n=3 rats per group). (**C**) Pancreatic lactate concentrations in Sham, AP, AAV-sh-NCOA4+ AP and AAV-sh-NC+ AP rats (n=3 rats per group). (**D**-**H**) Serum levels of amylase, lipase, IL-6, IL-1β, and TNF-α in Sham, AP, AAV-sh-NCOA4+ AP and AAV-sh-NC+ AP rats (n=3 rats per group). (**I**-**L**) Levels of glutathione (GSH), malondialdehyde (MDA), lipid peroxides, and ferrous iron in pancreatic tissues in Sham, AP, AAV-sh-NCOA4 + AP and AAV-sh-NC + AP rats (n=3 rats per group). (**M** and **N**) Western blot images and relative protein levels of NCOA4, FTH1, GPX4 and LC3 protein levels in pancreatic tissues from Sham, AP, AAV-sh-NCOA4 + AP and AAV-sh-NC + AP rats (n=3 rats per group). (**O**) NCOA4, FTH1 and GPX4 mRNA expressionlevels of Sham, AP, AAV-sh-NCOA4 + AP and AAV-sh-NC + AP rats (n=3 rats per group). (**P**) Representative TEM images of pancreas in Sham, AP, AAV-sh-NCOA4 + AP and AAV-sh-NC + AP rats. (**Q** and **R**) Western blot images and relative protein levels of NCOA4, FTH1, GPX4 and LC3 protein levels of AR42J cells in PBS (Con), caerulein (AP), si-NCOA4 + caerulein (si-NCOA4 + AP) and si-NC + caerulein (si-NC + AP) (n=3 biologically independent samples per group). (**S**) NCOA4, FTH1 and GPX4 mRNA expression levels of AR42J cells in Con, AP, si-NCOA4 + AP and si-NC + AP(n=3 biologically independent samples per group). (**T**-**X**) Representative images and quantification of JC-1, FeRhNOX-1 and DCFH-DA of AR42J cells in Con, AP, si-NCOA4 + AP and si-NC + AP (n=3 biologically independent samples per group). Statistical analyses: One-way ANOVA followed by Tukey's post hoc test in (B), (C), (D), (E), (F), (G), (H), (I), (J), (K), (L), (U), (W) and (X); Two-way ANOVA followed by Tukey's post hoc test in (N), (O), (R) and (S). Data are presented as mean ± SD. *$p < 0.05$; **$p < 0.01$; ***$p < 0.001$; ****$p < 0.0001$

AP-induced mitochondrial cristae loss and outer membrane rupture (Fig. 5Q).

In the AP model in vitro, compared with AP group, treatment with Fer-1 (Fer-1 + AP) significantly reduced the expressions of H3K18la, NCOA4, and LC3 II/I, while upregulating FTH1 and GPX4 (Fig. 6A-D), restored the MMP and lowered ferrous iron and ROS levels (Fig. 6E-I). Compared with AP group, Lac-Na treatment (Lac-Na + AP) elevated H3K18la, NCOA4 and LC3 II/I expressions, reduced FTH1 and GPX4 levels (Fig. 6A-D), increased intracellular ferrous iron and ROS levels, and further impaired MMP (Fig. 6E-I). Notably, these adverse effects induced by Lac-Na were largely reversed by Fer-1 co-treatment (Lac-Na + Fer-1 + AP) (Fig. 6A-I).

These findings suggest that NCOA4-mediated ferroptosis plays a key role in the progression of AP. Inhibition of ferroptosis led to decreased levels of lactate and H3K18la, alleviated pancreatic injury, and suppressed NCOA4-mediated ferroptosis. Conversely, lactate exacerbated pancreatic damage by promoting ferroptosis in the AP model.

NCOA4 Knockdown Suppresses Ferroptosis and Ameliorates AP

To elucidate the crucial role of NCOA4-mediated ferroptosis in AP, we constructed an AAV-sh-NCOA4 adeno-associated virus to knock down NCOA4 and subsequently established an AP rat model (The knockdown efficiency of AAV-sh-NCOA4-1 was shown in Figure S7). The results compared with the AP and AAV-sh-NC + AP groups, NCOA4 knockdown alleviated pancreatic tissue injury induced by AP (Fig. 7A-B), reduced the level of lactate (Fig. 7C), amylase (Fig. 7D), lipase (Fig. 7E), inflammatory factors (Fig. 7F-H), increased GSH levels (Fig. 7I), and decreased MDA, lipid peroxide, ferrous iron levels (Fig. 7J-L). NCOA4 knockdown markedly decreased the expression of NCOA4 and LC3II/I while increasing the expression of FTH1 and GPX4 (Fig. 7M-O). TEM observation revealed that compared with AP and AAV-sh-NC + AP groups, the mitochondrial damage of the pancreatic tissue in AAV-sh-NCOA4 + AP group rats was significantly ameliorated (Fig. 7P). In vitro AP model results demonstrated that siRNA-mediated silencing of NCOA4 (si-NCOA4) significantly reduced NCOA4 and LC3 II/I expression, while elevating FTH1 and GPX4 expression (Fig. 7Q-S). Furthermore, si-NCOA4 decreased intracellular ferrous iron and ROS levels and restored mitochondrial membrane potential (MMP) (Fig. 7T-X). Collectively, these findings suggest that inhibiting NCOA4 effectively alleviated ferroptosis, pancreatic injury and inflammation induced by AP.

Inhibiting NCOA4-mediated Ferroptosis Can Alleviate the Inflammatory and Tissue Damage Caused by Lactate in AP

To investigate the specific role of lactate in regulating NCOA4-mediated ferroptosis in AP, we administered the AAV-sh-NCOA4 virus, followed by Lac-Na pretreatment, and then established an in vivo AP rat model. Compared with Lac-Na + AP group, in AAV-sh-NCOA4 + Lac-Na + AP group, NCOA4 knockdown alleviated lactate-induced pancreatic injury (Fig. 8A-B), suppressed the increases in lactate (Fig. 8C), serum amylase (Fig. 8D), lipase (Fig. 8E), inflammatory cytokine levels (Fig. 8F-H), elevated GSH levels (Fig. 8I), and reduced pancreatic MDA, lipid peroxide, and ferrous iron levels (Fig. 8J-L), and attenuated Lac-Na-enhanced upregulation of NCOA4 and LC3 II/I expression and downregulation of GPX4 and FTH1 expression (Fig. 8M-O) promoted by Lac-Na pretreatment. TEM analysis confirmed these findings, demonstrating that NCOA4 knockdown restored the abnormal mitochondrial morphology induced by lactate (Fig. 8P). Furthermore, in the in vitro AP model, compared with AP and AP + si-NC group, in AP + si-NCOA4 group, siRNA-mediated NCOA4 silencing (si-NCOA4) reversed lactate-enhanced upregulation of NCOA4 and LC3 II/I and downregulation of FTH1 and GPX4 (Fig. 8Q-S) while reducing mitochondrial damage, ferrous iron accumulation, and ROS production (Fig. 8T-X). Collectively, these

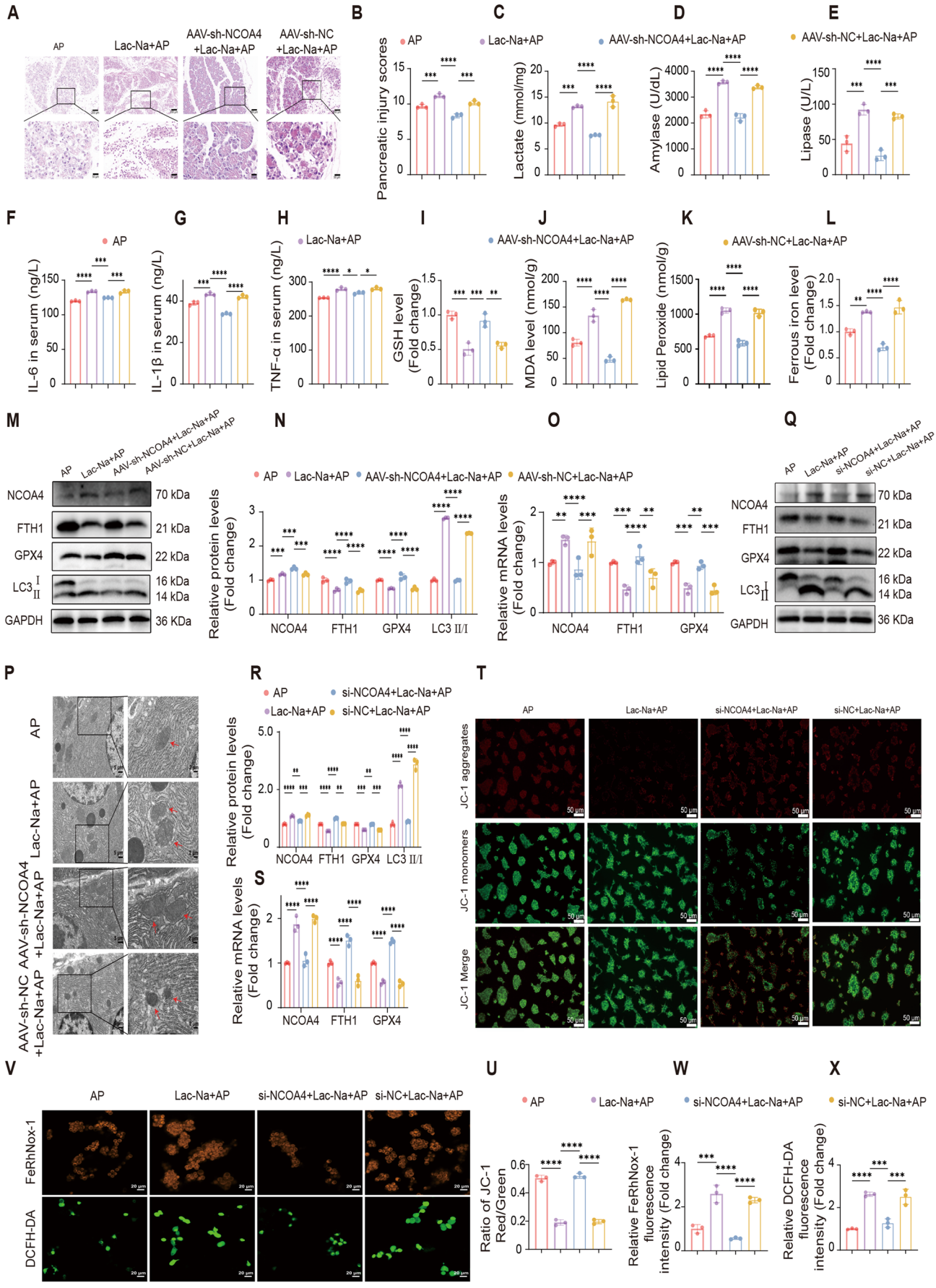

A
AP
Lac-Na+AP
AAV-sh-NCOA4 +Lac-Na+AP
AAV-sh-NC +Lac-Na+AP
B
Pancreatic injury scores
C
Lactate (mmol/mg)
D
Amylase (U/dL)
E
Lipase (U/L)
F
IL-6 in serum (ng/L)
G
IL-1β in serum (ng/L)
H
TNF-α in serum (ng/L)
I
GSH level (Fold change)
J
MDA level (nmol/g)
K
Lipid Peroxide (nmol/g)
L
Ferrous iron level (Fold change)
M
NCOA4
FTH1
GPX4
LC3 I/II
GAPDH
70 kDa
21 kDa
22 kDa
16 kDa
14 kDa
36 kDa
Relative protein levels (Fold change)
N
Relative mRNA levels (Fold change)
O
Q
si-NCOA4+Lac-Na+AP
si-NC+Lac-Na+AP
P
AAV-sh-NCOA4 +Lac-Na+AP
AAV-sh-NC +Lac-Na+AP
R
S
T
JC-1 aggregates
JC-1 monomers
JC-1 Merge
50 μm
V
FeRhNox-1
DCFH-DA
20 μm
U
Ratio of JC-1 Red/Green
W
Relative FeRhNox-1 fluorescence intensity (Fold change)
X
Relative DCFH-DA fluorescence intensity (Fold change)

Fig. 8 NCOA4 inhibition can rescue lactate promoted-ferroptosis, pancreatic inflammation and injury of AP (**A**–**B**) Representative pancreatic HE-stained images and injury scores in AP, sodium lactate+ AP (Lac-Na+ AP), AAV-sh-NCOA4+ sodium lactate+ AP (AAV-sh-NCOA4+ Lac-Na+ AP) and AAV-sh-NC+ sodium lactate+ AP (AAV-sh-NC+ Lac-Na+ AP) rats (n=3 rats per group). (**C**) Pancreatic lactate concentrations in AP, Lac-Na+ AP, AAV-sh-NCOA4+ Lac-Na+ AP and AAV-sh-NC+ Lac-Na+ AP rats (n=3 rats per group). (**D**–**H**) Serum amylase, lipase, IL-6, IL-1β and TNF-α levels in AP, Lac-Na+ AP, AAV-sh-NCOA4+ Lac-Na+ AP and AAV-sh-NC+ Lac-Na+ AP rats (n=3 rats per group). (**I**–**L**) Levels of glutathione (GSH), malondialdehyde (MDA), lipid peroxides, and ferrous iron in pancreatic tissues in AP, Lac-Na+ AP, AAV-sh-NCOA4+ Lac-Na + AP and AAV-sh-NC+ Lac-Na + AP rats (n=3 rats per group). (M and N) Western blot images and relative protein levels ofNCOA4, FTH1, GPX4 and LC3 in pancreatic tissues from AP, Lac-Na+ AP, AAV-sh-NCOA4+ Lac-Na+ AP and AAV-sh-NC+ Lac-Na+ AP rats (n=3 rats per group). (**O**) NCOA4, FTH1 and GPX4 mRNA expression of in pancreatic tissues from AP, Lac-Na+ AP, AAV-sh-NCOA4+ Lac-Na+ AP and AAV-sh-NC+ Lac-Na+ AP rats. (**P**) Representative TEM images of pancreas in AP, Lac-Na+ AP, AAV-sh-NCOA4+ Lac-Na+ AP and AAV-sh-NC+ Lac-Na+ AP rats. (**Q** and **R**) Western blot images and relative protein levels of NCOA4, FTH1, GPX4 and LC3 protein levels of AR42J cells in caerulein (AP), sodium lactate+ caerulein (Lac-Na+ AP), si-NCOA4+ sodium lactate+ caerulein (si-NCOA4+ Lac-Na+ AP), si-NC+ sodium lactate+ caerulein (si-NC+ Lac-Na+ AP) group (n=3 biologically independent samples per group). (S) mRNA expression levels of NCOA4, FTH1, and GPX4 of AR42J cells in AP, sodium Lac-Na+ AP, si-NCOA4+ Lac-Na+ AP, si-NC+ Lac-Na+ AP group (n=3 biologically independent samples per group). (T-X) Representative images and quantification of JC-1, FeRhNOX-1 and DCFH-DA of AR42J cells in AP, Lac-Na+ AP, si-NCOA4+ Lac-Na+ AP, si-NC+ Lac-Na+ AP group (n=3 biologically independent samples per group). Statistical analyses: One-way ANOVA followed by Tukey's post hoc test in (B), (C), (D), (E), (F), (G), (H), (I), (J), (K), (L), (U), (W) and (X); Two-way ANOVA followed by Tukey's post hoc test in (N), (O), (R) and (S). Data are presented as mean ± SD. *p< 0.05; **p< 0.01; ***p< 0.001; ****p< 0.0001

results indicate that lactate promotes NCOA4-mediated ferroptosis, whereas inhibition of NCOA4 alleviates lactate-induced inflammation and tissue damage in AP.

In summary, increased lactate levels exacerbated tissue damage and inflammation in AP via a mechanism involving H3K18la upregulation, subsequent enhancement of NCOA4 transcription, and activation of NCOA4-mediated ferritinophagy and ferroptosis (Fig. 9).

Discussion

AP is a common and potentially life-threatening inflammatory disorder of the pancreas. Approximately 15%–20% of AP cases develop into severe AP, which can result in systemic inflammatory response syndrome (SIRS), multiple organ dysfunction, and varying degrees of long-term complications [1–4]. Notably, elevated lactate levels have been shown to positively correlate with disease severity and mortality in AP patients [12–17], suggesting that the progression of AP may be closely associated with lactate accumulation. However, the molecular mechanisms by which elevated lactate contributes to pancreatic injury during AP remain largely unclear.

In this study, we aimed to elucidate the role of lactate in the pathogenesis of AP. Previous studies have shown that in L-arginine-induced AP rats, serum levels of TNF-α and IL-6 were significantly elevated at 12 h and continued to increase at 48 h [45]– [46]. Additionally, iNOS activity and pancreatic MDA levels were markedly increased at 24 h and peaked at 48 h in this model [47]–[48]. Based on these previous findings, we selected 48 h as the endpoint for the L-arginine-induced AP model in this study. In the present study, our results demonstrated that lactate levels were significantly elevated in AP rats and were positively correlated with the severity of pancreatic inflammation and tissue injury. Exogenous lactate administration exacerbated pancreatic damage, inflammation, and ferroptosis, whereas inhibition of lactate production significantly alleviated these pathological alterations in AP.

As previously reported, lactate-derived lactylation of histone lysines regulates the transcription of downstream target genes, thereby modulating various biological processes, such as metabolic regulation, tumorigenesis and post-myocardial infarction remodeling [18–22, 49, 50]. In addition, lactate has been shown to influence inflammation through multiple pathways. In kidneys subjected to ischemia-reperfusion injury (IRI), lactate increases H4K12la expression, promoting the inflammatory response by upregulating NF-κB [49]. In type 2 diabetes mellitus, elevated lactate levels enhance H4K12la in macrophages, facilitating inflammatory infiltration [50]. Furthermore, a recent study has indicated that a potential link between lactate, histone lactylation, lung injury, inflammation, and ferroptosis [23]. Ferroptosis is a distinct form of iron-dependent cell death, characterized by an increased reliance of ROS production on ferroptosis substrates, with intracellular ROS oxidation surpassing the antioxidant capacity of GPX4, thereby disrupting redox homeostasis [25]. Previous studies have shown that ferroptosis plays a pivotal role in the progression of AP. Inhibiting ferroptosis suppresses the inflammatory response and alleviates tissue damage caused by AP [38, 39]. However, the regulatory relationship between lactate and ferroptosis in AP remains incompletely understood. Here, our results indicate that lactate increases both pan- and histone-lysine lactylation. H3K18la is enriched at the promoter region of the ferroptosis-related gene NCOA4, suggesting that H3K18la regulates NCOA4 transcription. Exogenous lactate treatment increased the expression of NCOA4 and LC3II/I, suppressed FTH1 and GPX4, and promoted ferroptosis. Conversely, inhibiting endogenous lactate production via

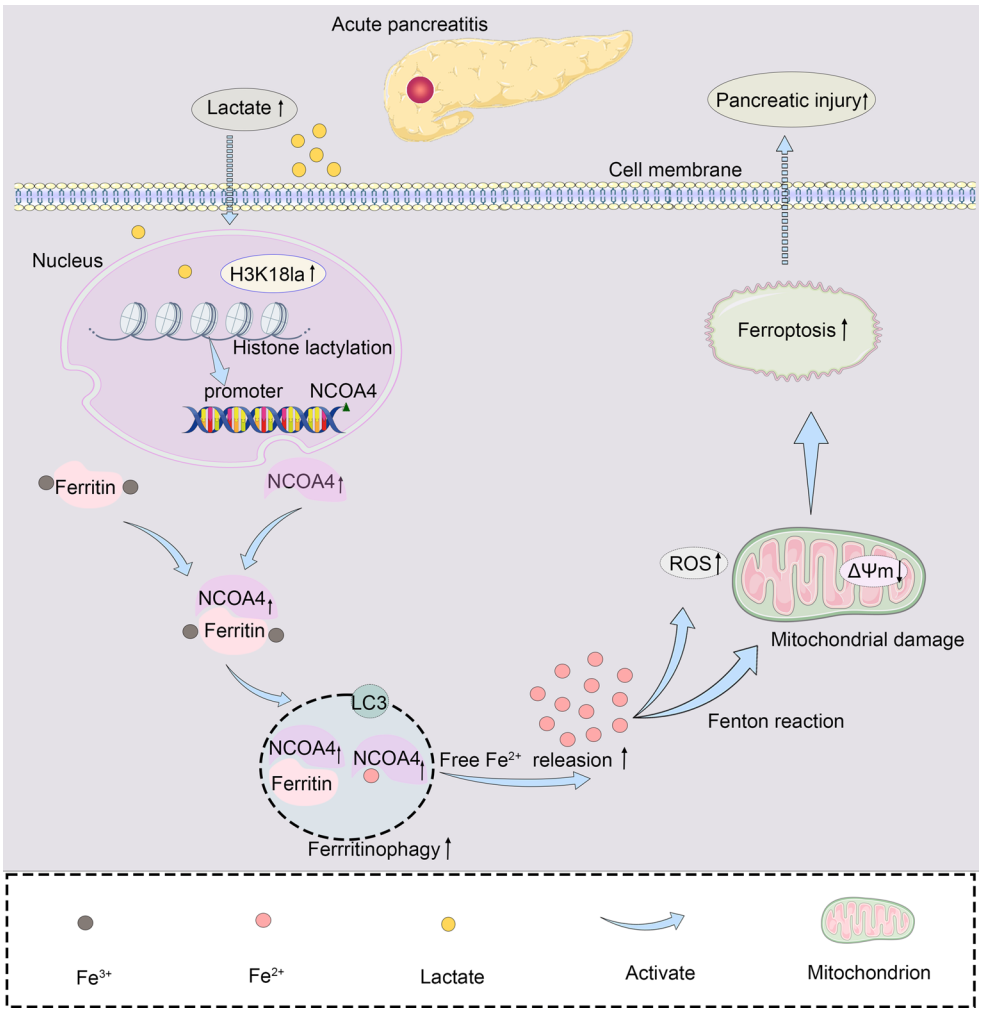


Fig. 9 Schematic illustration depicting the mechanism of H3K18la exacerbating AP via NCOA4-mediated ferroptosis

oxamate (OXA) produced opposite effects. As lactate levels increased, H3K18la and NCOA4 expression rose, while FTH1 and GPX4 levels decreased, indicating that lactate and H3K18 lactylation regulate NCOA4-mediated ferroptosis.

NCOA4 is a critical regulator of ferroptosis, and its involvement has been linked to the progression of various diseases [36, 37]. However, the role of NCOA4-mediated ferroptosis in acute pancreatitis (AP) remains poorly understood. In this study, we demonstrate that NCOA4-mediated ferroptosis contributes to pancreatic injury and inflammation in AP. Lactate promotes NCOA4-mediated ferroptosis, whereas inhibition of lactate production attenuates this process. Furthermore, NCOA4 knockdown alleviates ferroptosis and mitigates pancreatic inflammation and damage in AP. Additionally, NCOA4 knockdown effectively attenuates lactate-promoted ferroptosis and pancreatic injury in AP. We also employed AGK2, an inhibitor of the deacetylase SIRT2, to investigate its effect on H3K18la. Compared with the AP group, AGK2 did not increase the expression of H3K18la, H4K8la, or H4K12la in AP (Figure S8A-B), suggesting that SIRT2 may not function as a delactylase in AP. However, further experiments involving other deacetylases or H3K18 site mutants are necessary to confirm the role of H3K18la. Moreover, NCOA4 knockdown suppressed the expression of NCOA4 and increased GPX4 expression (Fig. 7M-S), while GPX4 overexpression enhanced GPX4 levels without affecting NCOA4 expression (Figure S9A-C). The combination of NCOA4 knockdown and GPX4 overexpression further elevated GPX4 expression, although this did not have statistical significance (Figure S9D-E). These findings suggested that NCOA4 might negatively regulate GPX4 expression.

Previous studies have shown that in sepsis-related acute lung injury (ALI), lactate induces ACSL4-dependent ferroptosis in alveolar epithelial cells through METTL3-mediated m^{6}A modification via the H3K18la/METTL3/ACSL4 axis [23]. Another study reported that lactate enhances H3K18la expression, thereby promoting ACSL4 upregulation and activating ACSL4-mediated ferroptosis during intervertebral disc degeneration [51].

In the present study, our results demonstrate that the overlapped results of the upregulated ferroptosis-related genes and the enrichment of H3K18la binding peaks of ferroptosis-related genes revealed that the downstream targeted gene of H3K18la was NCOA4, rather than ACSL4 or PTGS2. Our results demonstrate that lactate induces NCOA4-mediated ferroptosis and exacerbates pancreatic injury, which is driven by the axis of lactate-H3K18la-NCOA4 during AP.

In summary, the lactate–H3K18la–NCOA4 axis promotes iron and ROS accumulation, induces ferroptosis, and exacerbates pancreatic injury. NCOA4 knockdown inhibits AP-induced ferroptosis, alleviates pancreatic inflammation and damage, and attenuates the detrimental effects of lactate in AP. Lactate and H3K18la aggravate AP by modulating NCOA4-mediated ferroptosis. Systemic inhibition of lactate may affect energy metabolism, including cerebral function. For example, LDHA knockout-mediated reduction in brain lactate levels has been shown to promote depressive-like behaviors and decrease neuronal excitability in the dorsomedial prefrontal cortex in mice [52]. Additionally, systemic NCOA4 knockout may confer ferroptosis resistance, as NCOA4 deficiency leads to reduced ferroptosis in intestinal epithelium after radiotherapy [35]. Therefore, targeting NCOA4-mediated ferroptosis or controlling lactate levels with LDH inhibitors such as oxamate represents a promising therapeutic strategy for AP. However, given the dual role of lactate in energy metabolism, systemic lactate inhibition should be approached with caution. Our findings provide new insights for developing novel AP treatments targeting this mechanism.

Limitations of this Study

One limitation is the use of the rat pancreatic acinar cell line AR42J rather than primary pancreatic acinar cells for in vitro experiments. Although supplementary data from primary acinar cells are included (Figure S10) to enhance applicability, further validation in primary cells is warranted. Although lipid peroxidation was detected in pancreatic tissues across experimental groups, additional C11-BODIPY assays may be necessary to specifically assess lipid peroxidation in acinar cells in vitro. The absence of such markers may affect the robustness of our conclusions. And although we have demonstrated that lactate activates NCOA4-mediated ferroptosis by increasing the level of H3K18la, thereby exacerbating the pancreatic tissue damage and inflammation of AP. However, there are other viewpoints regarding the role of lactate in AP. Some studies suggest that lactate alleviates pancreatic injury and inflammation by inhibiting NF-κB activation [53]. Notably, the referenced study used a lactate concentration of 150 mM, administered to mice at 30 μL/g (0.5 g/kg), whereas our study employed a lactate dose of 2 g/kg in rats. This difference in lactate dosage may contribute to the divergent experimental outcomes. Furthermore, our results indicate that NCOA4 knockdown or ferroptosis inhibition significantly reduces lactate level in AP rats. We therefore speculate that there may be a positive feedback regulatory loop between lactate and ferroptosis mediated by NCOA4, which warrants further investigation in future studies.

Supplementary Information The online version contains supplementary material available at https://doi.org/10.1007/s10753-025-02361-x.

Author Contributions All authors contributed to the study conception and design. Material preparation, data collection and analysis were performed by Zi-Yu Han, Xue-Ying Ma, Shi-Ya Ma and Zhao-Jian Shen. The first draft of the manuscript was written by Zi-Yu Han, Xue-Ying Ma, Zhong-Hua Lu, Yun Sun, Wei-Li Yu and all authors commented on previous versions of the manuscript. All authors read and approved the final manuscript.

Funding This work was supported by the Natural Science Research Project of Colleges and Universities of Anhui Province (Grant No. 2024AH050800, 2024AH040107) and Research Fund of Anhui Institute of Translational Medicine (Grant No. 2023zhyx-C63).

Data Availability The datasets used and/or analysed during the current study are available from the corresponding author on reasonable request.

Declarations

Ethics Approval All animal experiments were approved by the Ethics Committee of Anhui Medical University.

Consent for Publish Not applicable.

Competing interests The authors declare no competing interests.

Open Access This article is licensed under a Creative Commons Attribution 4.0 International License, which permits use, sharing, adaptation, distribution and reproduction in any medium or format, as long as you give appropriate credit to the original author(s) and the source, provide a link to the Creative Commons licence, and indicate if changes were made. The images or other third party material in this article are included in the article's Creative Commons licence, unless indicated otherwise in a credit line to the material. If material is not included in the article's Creative Commons licence and your intended use is not permitted by statutory regulation or exceeds the permitted use, you will need to obtain permission directly from the copyright holder. To view a copy of this licence, visit http://creativecommons.org/licenses/by/4.0/.

References

1. Mederos, M.A., H.A. Reber, and M.D. Girgis. 2021. Acute pancreatitis: A review. *JAMA* 325: 382–390. https://doi.org/10.1001/jama.2020.20317.
2. Gardner, T.B., and Acute Pancreatitis. 2021. *Annals of Internal Medicine* 174: ITC17–ITC32. https://doi.org/10.7326/AITC202102160.
3. Trikudanathan, G., C. Yazici, A. Evans Phillips, and C.E. Forsmark. 2024. Diagnosis and management of acute pancreatitis. *Gastroenterology* 167: 673–688. https://doi.org/10.1053/j.gastro.2024.02.052.
4. Petrov, M.S., and D. Yadav. 2019. Global epidemiology and holistic prevention of pancreatitis. *Nature Reviews. Gastroenterology & Hepatology* 16: 175–184. https://doi.org/10.1038/s41575-018-0087-5.
5. Boxhoorn, L., R.P. Voermans, S.A. Bouwense, M.J. Bruno, R.C. Verdonk, M.A. Boermeester, et al. 2020. Acute pancreatitis. *Lancet* 396: 726–734. https://doi.org/10.1016/S0140-6736(20)31310-6.
6. van Dijk, S.M., N.D.L. Hallensleben, H.C. van Santvoort, P. Fockens, H. van Goor, M.J. Bruno, et al. 2017. Acute pancreatitis: Recent advances through randomised trials. *Gut* 66: 2024–2032. https://doi.org/10.1136/gutjnl-2016-313595.
7. Umapathy, C., A. Raina, S. Saligram, G. Tang, G. Papachristou, M. Rabinovitz, et al. 2016. Natural history after acute necrotizing pancreatitis: A large US tertiary care experience. *Journal of Gastrointestinal Surgery* 20: 1844–1853. https://doi.org/10.1007/s11605-016-3264-2.
8. Hart, P.A., D. Bradley, D.L. Conwell, K. Dungan, S.G. Krishna, K. Wyne, et al. 2021. Diabetes following acute pancreatitis. *The Lancet Gastroenterology & Hepatology* 6 (8): 668–675. https://doi.org/10.1016/S2468-1253(21)00019-4.
9. Huang, W., D. de la Iglesia-García, I. Baston-Rey, C. Calviño-Suarez, J. Lariño-Noia, and J. Iglesias-Garcia. 2019. Exocrine pancreatic insufficiency following acute pancreatitis: Systematic review and meta-analysis. *Digestive Diseases and Sciences* 64: 1985–2005. https://doi.org/10.1007/s10620-019-05568-9.
10. Beij, A., R.C. Verdonk, H.C. van Santvoort, E. de-Madaria, and R.P. Voermans. 2025. Acute pancreatitis: An update of evidence-based management and recent trends in treatment strategies. *United European Gastroenterology Journal* 13: 97–106. https://doi.org/10.1002/ueg2.12743.
11. Palumbo, R., and K.M. Schuster. 2024. Contemporary management of acute pancreatitis: What you need to know. *The Journal of Trauma and Acute Care Surgery* 96: 156–165. https://doi.org/10.1097/TA.0000000000004143.
12. Shu, W., J. Wan, J. Chen, W. He, Y. Zhu, N. Lu, et al. 2019. Elevated arterial lactate level as an independent risk factor for pancreatic infection in moderately severe acute pancreatitis. *Pancreatology* 19: 653–657. https://doi.org/10.1016/j.pan.2019.06.001.
13. Xu, S.X., N.Z. Wang, G.H. Yao, Y.B. Ding, and C.F. Xu. 2024. Elevated venous lactate level as an early predictive marker of organ failure in acute pancreatitis: A retrospective study. *European Review for Medical and Pharmacological Sciences* 28: 2179–2185. https://doi.org/10.26355/eurrev-202403-35721.
14. Zeng, Z., R. Huang, H. Linn, H. Peng, J. Luo, and N. Ding. 2024. Serum lactate is an indicator for short-term and long-term mortality in patients with acute pancreatitis. *Digestive Diseases and Sciences* 69: 2223–2234. https://doi.org/10.1007/s10620-024-08419-4.
15. Liu, Q., H.L. Zheng, M.M. Wu, Q.Z. Wang, S.J. Yan, M. Wang, et al. 2022. Association between lactate-to-albumin ratio and 28-days all-cause mortality in patients with acute pancreatitis: A retrospective analysis of the MIMIC-IV database. *Frontiers in Immunology* 13: 1076121. https://doi.org/10.3389/fimmu.2022.1076121.
16. Tian, F., H. Li, L. Wang, B. Li, M. Aibibula, H. Zhao, et al. 2020. The diagnostic value of serum C-reactive protein, procalcitonin, interleukin-6 and lactate dehydrogenase in patients with severe acute pancreatitis. *Clinica Chimica Acta* 510: 665–670. https://doi.org/10.1016/j.cca.2020.08.029.
17. Huang, D.N., H.J. Zhong, Y.L. Cai, W.R. Xie, and X.X. He. 2022. Serum lactate dehydrogenase is a sensitive predictor of systemic complications of acute pancreatitis. *Gastroenterology Research and Practice* 2022. https://doi.org/10.1155/2022/1131235.
18. Zhang, D., Z. Tang, H. Huang, G. Zhou, C. Cui, Y. Weng, et al. 2019. Metabolic regulation of gene expression by histone lactylation. *Nature* 574: 575–580. https://doi.org/10.1038/s41586-019-1678-1.
19. Yu, J., P. Chai, M. Xie, S. Ge, J. Ruan, X. Fan, et al. 2021. Histone lactylation drives oncogenesis by facilitating m6A reader protein YTHDF2 expression in ocular melanoma. *Genome Biology* 22: 85. https://doi.org/10.1186/s13059-021-02308-z.
20. Irizarry-Caro, R.A., M.M. McDaniel, G.R. Overcast, V.G. Jain, T.D. Troutman, and C. Pasare. 2020. TLR signaling adapter BCAP regulates inflammatory to reparatory macrophage transition by promoting histone lactylation. *Proceedings of the National Academy of Sciences of the United States of America* 117: 30628–30638. https://doi.org/10.1073/pnas.2009778117.
21. Wang, N., W. Wang, X. Wang, G. Mang, J. Chen, X. Yan, et al. 2022. Histone lactylation boosts reparative gene activation post-myocardial infarction. *Circulation Research* 131: 893–908. https://doi.org/10.1161/CIRCRESAHA.122.320488.
22. Pan, R.Y., L. He, J. Zhang, X. Liu, Y. Liao, J. Gao, et al. 2022. Positive feedback regulation of microglial glucose metabolism by histone H4 lysine 12 lactylation in alzheimer's disease. *Cell Metab* 34: 634648. https://doi.org/10.1016/j.cmet.2022.02.013.
23. Wu, D., C.B. Spencer, L. Ortoga, H. Zhang, and C. Miao. 2024. Histone lactylation-regulated METTL3 promotes ferroptosis via m6A-modification on ACSL4 in sepsis-associated lung injury. *Redox Biology* 74: 103194. https://doi.org/10.1016/j.redox.2024.103194.
24. Lee, P.J., and G.I. Papachristou. 2019. New insights into acute pancreatitis. *Nature Reviews Gastroenterology & Hepatology* 16: 479–496. https://doi.org/10.1038/s41575-019-0158-2.
25. Tang, D., X. Chen, R. Kang, and G. Kroemer. 2021. Ferroptosis: Molecular mechanisms and health implications. *Cell Research* 31: 107–125. https://doi.org/10.1038/s41422-020-00441-1.
26. Chen, X., R. Kang, G. Kroemer, and D. Tang. 2021. Ferroptosis in infection, inflammation, and immunity. *Journal of Experimental Medicine* 218: e20210518. https://doi.org/10.1084/jem.20210518.
27. Zhou, B., J. Liu, R. Kang, D.J. Klionsky, G. Kroemer, and D. Tang. 2020. Ferroptosis is a type of autophagy-dependent cell death. *Seminars in Cancer Biology* 66: 89–100. https://doi.org/10.1016/j.semcancer.2019.03.002.
28. Gao, M., P. Monian, Q. Pan, W. Zhang, J. Xiang, and X. Jiang. 2016. Ferroptosis is an autophagic cell death process. *Cell Research* 26: 1021–1032. https://doi.org/10.1038/cr.2016.95.
29. Chen, X., C. Yu, R. Kang, G. Kroemer, and D. Tang. 2021. Cellular degradation systems in ferroptosis. *Cell Death and Differentiation* 28: 1135–1148. https://doi.org/10.1038/s41418-020-00728-1.
30. Mancias, J.D., X. Wang, S.P. Gygi, J.W. Harper, and A.C. Kimmelman. 2014. Quantitative proteomics identifies NCOA4 as the cargo receptor mediating ferritinophagy. *Nature* 509 (7498): 105–109. https://doi.org/10.1038/nature13148.
31. Hou, W., Y. Xie, X. Song, X. Sun, M.T. Lotze, H.J. Zeh, et al. 2016. Autophagy promotes ferroptosis by degradation of ferritin.

Autophagy 12: 1425–1428. https://doi.org/10.1080/15548627.2016.1187366.
32. Qin, X., J. Zhang, B. Wang, G. Xu, X. Yang, Z. Zou, et al. 2021. Ferritinophagy is involved in the zinc oxide nanoparticles-induced ferroptosis of vascular endothelial cells. *Autophagy* 17: 4266–4285. https://doi.org/10.1080/15548627.2021.1911016.
33. Jin, X., C. Jiang, Z. Zou, H. Huang, X. Li, S. Xu, et al. 2023. Ferritinophagy in the etiopathogenic mechanism of related diseases. *Journal of Nutritional Biochemistry* 117: 109339. https://doi.org/10.1016/j.jnutbio.2023.109339.
34. He, J., Z. Li, P. Xia, A. Shi, X. FuChen, J. Zhang, et al. 2022. Ferroptosis and ferritinophagy in diabetes complications. *Molecular Metabolism* 60. https://doi.org/10.1016/j.molmet.2022.101470.
35. Zhou, H., Y.L. Zhou, J.A. Mao, L.F. Tang, J. Xu, Z.X. Wang, et al. 2022. NCOA4-mediated ferritinophagy is involved in ionizing radiation-induced ferroptosis of intestinal epithelial cells. *Redox Biology* 55: 102413. https://doi.org/10.1016/j.redox.2022.102413.
36. Li, K., B. Chen, A. Xu, J. Shen, K. Li, K. Hao, et al. 2022. TRIM7 modulates NCOA4-mediated ferritinophagy and ferroptosis in glioblastoma cells. *Redox Biology* 56: 102451. https://doi.org/10.1016/j.redox.2022.102451.
37. Huang, G., Y. Cai, M. Ren, X. Zhang, Y. Fu, and R. Cheng et al. 2024. Salidroside sensitizes Triple-negative breast cancer to ferroptosis by SCD1-mediated lipogenesis and NCOA4-mediated ferritinophagy. *Journal of Advanced Research* 29. https://doi.org/10.1016/j.jare.2024.09.027. S2090-1232(24)00429-6.
38. Ma, D., C. Li, P. Jiang, Y. Jiang, J. Wang, and D. Zhang. 2021. Inhibition of ferroptosis attenuates acute kidney injury in rats with severe acute pancreatitis. *Digestive Diseases and Sciences* 66: 483–92. https://doi.org/10.1007/s10620-020-06225-2.
39. Meng, Y.T., Y. Zhou, P.Y. Han, and H.B. Ren. 2023. Ferroptosis inhibition attenuates inflammatory response in mice with acute hypertriglyceridemic pancreatitis. *World Journal of Gastroenterology* 29: 2294–2309. https://doi.org/10.3748/wjg.v29.i15.2294.
40. Li, H., Y. Lin, L. Zhang, J. Zhao, and P. Li. 2022. Ferroptosis and its emerging roles in acute pancreatitis. *Chinese Medical Journal (Engl)* 135: 2026–2034. https://doi.org/10.1097/CM9.0000000000002096.
41. Toma, H., J. Winston, M.A. Micci, M. Shenoy, and P.J. Pasricha. 2020. Nerve growth factor expression is up-regulated in the rat model of L-arginine-induced acute pancreatitis. *Gastroenterology* 119: 1373–1381. https://doi.org/10.1053/gast.2000.19264.
42. Schmidt, J., K. Lewandrowsi, A.L. Warshaw, C.C. Compton, and D.W. Rattner. 1992. Morphometric characteristics and homogeneity of a new model of acute pancreatitis in the rat. *International Journal of Pancreatology* 12: 41–51. https://doi.org/10.1007/BF02927069.
43. Taylor, S.C., K. Nadeau, M. Abbasi, C. Lachance, M. Nguyen, and J. Fenrich. 2019. The ultimate qPCR experiment: Producing publication quality, reproducible data the first time. *Trends in Biotechnology* 37: 761–774. https://doi.org/10.1016/j.tibtech.2018.12.002.
44. Shao, J., Z. Bai, L. Zhang, and F. Zhang. 2022. Ferrostatin-1 alleviates tissue and cell damage in diabetic retinopathy by improving the antioxidant capacity of the Xc–GPX4 system. *Cell Death Discovery* 8. https://doi.org/10.1038/s41420-022-01141-y.
45. Takacs, T., L. Czako, K. Jarmay, G. Farkas Jr., Y. Mandi, and J. Lonovics. 1996. Cytokine level changes in L-arginine-induced acute pancreatitis in rat. *Acta Physiologica Hungarica* 84: 147–156.
46. Czako, L., T. Takacs, I.S. Varga, D.Q. Hai, L. Tiszlavicz, P. Hegyi, Y. Mandi, B. Matkovics, and J. Lonovics. 2000. The pathogenesis of L-arginine induced acute necrotizing pancreatitis: Inflammatory mediators and endogenous cholecystokinin. *Journal De Physiologie (Paris)* 94: 43–50. https://doi.org/10.1016/s0928-4257(99)00104-7.
47. Varga, I.S., B. Matkovics, D.Q. Hai, M. Kotorman, T. Takacs, and M. Sasvari. 1997. Lipid peroxidation and antioxidant system changes in acute L-arginine pancreatitis in rats. *Acta Physiologica Hungarica* 85: 129–138.
48. Czako, L., T. Takacs, I.S. Varga, L. Tiszlavicz, D.Q. Hai, P. Hegyi, B. Matkovics, and J. Lonovics. 1998. Involvement of oxygen-derived free radicals in L-arginine-induced acute pancreatitis. *Digestive Diseases and Sciences* 43: 1770–1777. https://doi.org/10.1023/a:1018839821176.
49. Wang, Y., H. Li, S. Jiang, D. Fu, X. Lu, M. Lu, Y. Li, D. Luo, K. Wu, Y. Xu, G. Li, Y. Zhou, Y. Zhou, W. Chen, Q. Liu, and H. Mao. 2024. The glycolytic enzyme PFKFB3 drives kidney fibrosis through promoting histone lactylation-mediated NF-κB family activation. *Kidney International* 106: 226–240. https://doi.org/10.1016/j.kint.2024.04.016.
50. Ma, X.M., K. Geng, P. Wang, Z. Jiang, B.Y. Law, and Y. Xu. 2024. MCT4-dependent lactate transport: A novel mechanism for cardiac energy metabolism injury and inflammation in type 2 diabetes mellitus. *Cardiovascular Diabetology* 23. https://doi.org/10.1186/s12933-024-02178-2.
51. Sun, K., Y. Shi, C. Yan, S. Wang, L. Han, F. Li, X. Xu, Y. Wang, J. Sun, Z. Kang, and J. Shi. 2025. Glycolysis-derived lactate induces ACSL4 expression and lactylation to activate ferroptosis during intervertebral disc degeneration. *Advanced Science* 12 (21). https://doi.org/10.1002/advs.202416149.
52. Yao, S., M.D. Xu, Y. Wang, S.T. Zhao, J. Wang, G.F. Chen, W.B. Chen, J. Liu, G.B. Huang, W.J. Sun, Y.Y. Zhang, H.L. Hou, L. Li, and X.D. Sun. 2023. Astrocytic lactate dehydrogenase A regulates neuronal excitability and depressive-like behaviors through lactate homeostasis in mice. *Nature Communications* 14 (1): 729. https://doi.org/10.1038/s41467-023-36209-5.
53. Hoque, R., A. Farooq, A. Ghani, F. Gorelick, and W.Z. Mehal. 2014. Lactate reduces liver and pancreatic injury in Toll-like receptor- and inflammasome-mediated inflammation via GPR81-mediated suppression of innate immunity. *Gastroenterology* 146: 1763–1774. https://doi.org/10.1053/j.gastro.2014.03.014.

Publisher's Note Springer Nature remains neutral with regard to jurisdictional claims in published maps and institutional affiliations.